Biomass and Bioenergy 197 (2025) 107843

Contents lists available at ScienceDirect

Biomass and Bioenergy

journal homepage: www.elsevier.com/locate/biombioe

A novel approach for biopitch-derived carbon foams: Combining mesoporous SBA-15 silica hard-templating method and chemical activation to modify the characteristics

Adife Şeyda Yargıç *, Gamze Gündüz Meriç, Yunus Dolaş, Nurgül Özbay

Chemical Engineering Department, Engineering Faculty, Gulumbe Campus, Bilecik Seyh Edebali University, 11100, Bilecik, Türkiye

ARTICLE INFO

Keywords:
Biopitch
Carbon foam
Chemical activation
Hard-template SBA-15
Hornbeam sawdust

ABSTRACT

This research aims to develop low-cost bio-based carbon foams, one of the newest forms of carbon that can be utilized in adsorption, catalytic reactions or thermal insulation applications by recycling hornbeam sawdust. Pyrolysis, biopitch synthesis, foaming, templating, carbonization, and activation processes were integrated to convert industrial waste sawdust into carbon foam with controllable properties. A strategy was followed to determine the impact degree of the template contribution and the chemical activation on the three-dimensional hierarchically arranged porous carbon foam production by regular and homogeneous foaming of the biopitch. The feasibility of obtaining foams with high surface area, consisting of meso- and micro-porous channels and macro-porous cores, and having a self-organized hierarchical structure was investigated when SBA-15 was employed as a hard template. Carbon foams with inferior thermal conductivity (0.25 W/m.K) and high strength (>1.5 MPa) were developed that have the potential to be utilized in thermal insulation applications. In light of the characterization results, it was concluded that carbon foams could attain the standard of being thermal insulation material based on the thermal conductivity coefficient measurements, and bio-based carbon foams additionally fulfill the adsorbent or catalyst support requirements in their respective fields of application. To illustrate the modifiable nature of material properties in the production process of carbon foam, it is absolutely critical to compare the template approach and chemical activation procedures. In conclusion, by highlighting clean production actions that utilize biomass as a superior option to fossil-based raw materials, it will be possible to contribute to the design of operating circumstances that adopt sustainable environmental awareness.

1. Introduction

Carbon foams (*CFs*) have attracted much curiosity due to their low cost, unique 3D porous, and ultra-lightweight structures. Large external surface area, low density, high mechanical compressive strength, compatibility with graphitic structure, high thermal conductivity, porous structure, high electrical conductivity, resistance to high temperatures, affordability, shapeability according to the intended area of use, and open cell structure are just a few of the advantageous properties of carbon foam. Carbon foam is also an excellent carbonaceous material for thermal applications because of its tailorable thermal conductivity properties [1–3]. The thermal properties of carbon foams are dependent on the morphology of their structure [4–6]. Many porous carbon materials, such as carbon nanotubes, graphite foams (*GF*), graphene aerogels, and metal foams including copper, iron, nickel, or aluminum with superior thermal conductivity, have been available. Porous carbonaceous materials have been noted for their excellent heat transfer performance [7]. Carbon foams are new-generation porous carbon materials and have numerous uses in a wide range of industries, including energy storage, water treatment, electrical and thermal conductivities, heat sinks, sound and electromagnetic wave absorption, vibration damping, fire resistance, etc. [8]. With their unique properties, they can be employed as adsorbents in sorption-based separation, as catalyst supports in catalytic reactions, as heat sinks in high-temperature thermal insulation, as shielding materials against electromagnetic interference, as construction materials for light fire-resistant structures in shipbuilding, and also as electrode and supercapacitor materials [9–17].

Many different feedstocks and techniques have been used to produce carbon foams. According to the literature, pitches generated from coal

* Corresponding author.
E-mail addresses: seyda.guler@bilecik.edu.tr, aseydaguler@gmail.com (A.Ş. Yargıç).

https://doi.org/10.1016/j.biombioe.2025.107843
Received 18 November 2024; Received in revised form 24 March 2025; Accepted 25 March 2025
Available online 31 March 2025
0961-9534/© 2025 Elsevier Ltd. All rights are reserved, including those for text and data mining, AI training, and similar technologies.

and petroleum are widely used in the manufacturing of commercial carbon foam [18,19]. The production of graphitic foam from coal tar-based mesophase pitch at high pressure and temperature was performed in 2007 [20]. Furthermore, bituminous coal was heat-treated at various pressure and temperature levels to produce graphitic porous foam [21]. Template approaches were used to generate reticulated graphitic foams [11,22,23]. However, the development of porous carbonaceous materials from biomass feedstocks has attracted more attention recently [24]. Research on using renewable raw materials for this purpose is therefore progressing at a rapid pace [25,26]. Nonetheless, research on the direct production of carbon foams from biomass feedstocks is lacking. The pyrolysis of olive stones at 500 °C and 1.0 MPa in a mixture of inert gas and water vapor was shown by Rios et al. [27] to produce carbon foam, however, the feedstock was not entirely transformed into foam. Smith et al. [28] showed that xylan could foam at a rate of 190 °C/s and ambient pressure; however, they found that lignin and cellulose either did not foam at all or only very little. The biomass liquefaction process was shown to be viable for producing carbon foam [29–31], and more recently, studies have concentrated on producing foam from the slow pyrolysis products of biomass [32,33].

Various investigations have been conducted on the carbon foams' thermal conductivities. Carbon foams were derived by these researchers from various precursors like coal, agriculture-related goods, and petroleum. They promote thermal conductivity by applying a variety of chemical substances to resources [34]. All kinds of biological organics, metabolites, and their natural derivatives are referred to as biomass materials. Biomass is definitely a great source to produce carbon compounds as a carbon precursor. Agricultural sources produce biomasses in large quantities all over the world. These biomasses are utilized in part to generate energy [35,36]. Also, agricultural residues have been used for the production of carbon foams, that find applications in thermal insulation, electromagnetic interference shielding, fire-resistant lightweight structures, etc. [37,38]. Preparation of high surface area activated carbon foams from various sources such as sawdust [8], wheat straw [39], cornstalk [40], potato waste [41], cotton [42], coffee ground [43], banana peel [44], etc. have been informed in the literature. Also, grapefruit peel [45], black pine [46], cotton wool [47], bamboo fiber [48], olive leaves [49], corn straw [50], cornstalk-derived materials [51], and other biomass carbon sources have been used to produce high-performance thermal conductivities.

Studies on the synthesis of carbonaceous materials have advanced in the modern period due to developments in technology. Alternative renewable resources for bio-based materials production are essential to prevent environmental problems. The production of carbon foam from biomass-based biopitch as a viable alternative to fossil-based pitch was investigated within the parameters of this study. This method has several advantages over other methods for producing carbon foam, such as the absence of harsh chemicals, feedstock flexibility, and added environmental benefits from using sustainable biomass waste feedstocks. Sawdust is a fine particle of wood that haven as a by-product of the wood processing industry. The use of sawdust for the formation of carbon foams from a liquefaction process was applied by several researchers [29,31,52]. Instead of this, a technique called vacuum distillation was carried out in this study to separate the aromatic component of the tars generated from the slow pyrolysis of biomass to produce biopitch. Then, carbon foam was generated by the foaming process, which used biopitch in a high-temperature/pressure reactor. The template method is an effective way to prepare carbon foams with regular morphology and regular pore structure. The second method, which encompassed the most notable originality of the study, involved combining biopitch with a hard-silica template before the foaming stage. After these processes, the effect of the activation process when using potassium hydroxide on the structure of the foams was investigated. The mechanical as well as physical characteristics of the bio-based carbon foams were also examined. The thermal conductivities of carbon foams were measured and this study analyzed their potential as insulation materials. The utilization of chemical activation and the template approach for carbon foam production based on biopitch had received no attention in the literature. The aim of skillfully applied foaming and activation procedures utilizing waste hornbeam sawdust was to enhance carbon foams' structural durability or porosity by adding templates to the foaming medium. The foaming of hornbeam sawdust biopitch via the template-assisted method in a high-temperature/pressure reactor and chemical activation techniques were used as the foundation for producing bio-based carbon foams. The carbon foams developed in this study are expected to be utilized as adsorbent, catalyst support, or thermal insulation material in the future due to their broad range of features.

2. Materials and methods

2.1. Characteristics of raw material

A lumber-processing plant in Eskişehir (Turkey) supplied the hornbeam tree waste sawdust (*HS*), which was further air-dried in the laboratory to create *CFs*. The bulk density and average particle size of the raw material were determined to be 0.26 g/cm^3 and 0.497 mm, respectively, after diminishing particle size employing the Armfield FT-7A mill. Then, preliminary and structural analysis was employed to identify the contents of *HS* as moisture (5.72 wt%, ASTM E 871-82), volatile matter (85.21 wt%, ASTM E 872-82), ash (0.45 wt%, ASTM D 1102-84), fixed carbon (8.62 wt%, ASTM E 870-82), extractive material (0.72 wt%, ASTM D 1107-96), holocellulose (67.92 wt%, TS 4431), lignin (30.92 wt%, ASTM D 1106-96), hemicellulose (32.58 wt%), and cellulose (35.34 wt%). The manufacture of tar and biopitch was facilitated by hornbeam sawdust's high volatile (85.21 %) and low ash (0.45 %) compositions. The high levels of phenolic substances in *HS*'s composition were indicated by the material's significant lignin concentration of 30.92 %. The high amount of ash with mineral substances in the biomass structure increases the waste cost and affects the thermal degradation efficiency. The amount of volatile matter is directly related to the tar yield and indicates the presence of condensable/non-condensable gases when the biomass is heated. For notable tar yield, pyrolysis is favored on biomass with a high volatile matter quantity. It is suggested to use tar, which is rich in phenolic compounds, to produce biopitch. The biomass to be selected in this context should contain lignin, which will enable the formation of phenolic compounds after thermal decomposition. Setaram Thermo analyzer Labsys Evo was implemented to examine the thermal behavior of *HS* in the 20–1000 °C temperature range, and the Leco CNH628-S628 elemental analyzer was utilized in the ultimate analysis to identify the CHN quantities at 950 °C. For tar, biopitch, and carbon foam preparation, lignin (30.92 wt%) and elemental carbon (45.99 %) quantities of sawdust were crucial. Following the findings of the ultimate analysis, the higher heating value (HHV) of *HS* was specified to be 16.33 MJ/kg. The TGA thermal curve of the raw material indicated that the severe drop in mass occurred up to nearly 550 °C, following the degradation and elimination of the cellulose and hemicellulose polymer compounds, which are contributing to the generation of volatile substances. Attenuated total reflectance-Fourier transform infrared (ATR-FTIR) spectroscopy (PerkinElmer Spectrum 100) analysis was applied to recognize the functional groups of *HS* in the wavenumber region of 4000-400 cm^{-1} with a resolution of 4 cm^{-1} after 100 scans. The peaks of C-H, -OH, C=C, C=O, C–O stretching or bending (asymmetric and symmetric) vibrations indicating aliphatic/olefinic/aromatic structures and phenol, alcohol, carboxylic acid, ester, ether, aldehyde, and ketone functional groups in the chemical structure of the lignocellulosic-containing *HS* precursor were detected in the FT-IR spectrum. To deeper comprehend the surface morphology under Zeiss Supra VP 40 scanning electron microscope (SEM), the raw material was platinum-coated using Quorum Q 150 R ES DC Sputter. The SEM image of the *HS* revealed that it had a non-porous fibrous structure. In our prior studies [53,54], the whole findings of the

biomass precursor analysis were critically evaluated.

2.2. Pyrolysis and characteristics of pyrolysis tar

The heating rate and reaction time in the slow pyrolysis were configured to 10 °C/min and 20 min, respectively. The thermochemical conversion was performed in the Heinze reactor at 400 °C under a static condition. The experimental methodology was comprehensively detailed in our related articles [29,32,53]. Calculation procedures were undertaken on a dry ash-free basis to find the amount of the pyrolysis products, and an average of three tests was computed. The yields of solid and gaseous products were 30.32 % and 22.37 %, respectively. The tar (*HS*$_{@400°C}$) yield to be used in the manufacturing of biopitch was identified as 19.95 %, even though the pyrolysis liquid product contained 27.36 % acidic aqueous phase. Since lignin in the raw material's structure decomposes at greater temperatures than cellulose, it is known that a high lignin content results in a substantial amount of solid products. Characteristics of pyrolytic oil (*HS*$_{@400°C}$) clarified by employing PerkinElmer Spectrum 100 Fourier transform infrared spectroscopy (FT-IR), Varian Mercury 300 MHz nuclear magnetic resonance spectroscopy (^{1}H NMR), Shimadzu GC-2010 Plus gas chromatography/mass spectroscopy (GC/MS), and Leco CHN628-S628 elemental analyzer were discussed in a prior research paper [53]. The elemental analysis revealed that the tar possessed an increased calorific value (24.82 MJ/kg) and a carbon amount (59.94 %) than hornbeam sawdust. The oxygen ratio of the tar produced by pyrolysis diminished while the carbon content improved, as indicated by O/C ratios estimated as 0.71 and 0.36 for *HS* and *HS*$_{@400°C}$, respectively. FT-IR analysis confirmed that the tar structure mirrored the chemical composition of the lignocellulosic *HS*, which included several organic components such as aliphatic, olefinic, and aromatic compounds. Carbohydrates are chemical compounds generated when the raw material's primary constituents of cellulose and hemicellulose break down. Guaiacol, syringol, and hydroxy phenols are produced via lignin decomposition. It was noticed that the principal peaks (with areas of at least 10 %) in the GC/MS chromatogram of *HS*$_{@400°C}$ attributed to phenolic substances involving phenol, 2-methyl-phenol, 4-methyl-phenol, 2,4-dimethyl-phenol, 2-ethyl-phenol, 3-ethyl-phenol, 3-ethyl-5-methyl-phenol, 4-propyl-phenol, and 3,4,5-trimethyl-phenol. The tar also entailed furfural and furan compounds derived from lignin since the raw material (*HS*) was lignocellulosic. The wood-based tar had an aromatic and conjugated olefinic content of 16.45 % determined by the chemical shift values of varied hydrogen species defined from the ^{1}H NMR spectrum in the range of 9.0–6.0 ppm because it contained a significant amount of phenolic molecules. Related components like carboxylic acids, ketones, aldehydes, and phenolic compounds can be identified in the tars derived from lignocellulosic sources. The content of phenols and unconjugated olefins (between the chemical shift range of 6.0 and 4.0 ppm) was also 20.10 %, while the total aliphatic content, determined in the chemical shift range of 3.0–0.5 ppm, was 51.77 % [55]. The percentage of ring-binding methylene, methoxy, and methyl protons was 10.87 % in the 4.0–3.0 ppm region of the ^{1}H NMR spectrum. The significant fraction (8.51 %) in the range of 1.5–1.0 ppm indicated the existence of γ or further alkyl groups (CH_3) linked to the aromatic ring in the tar and paraffinic CH_3 groups [29].

2.3. Biopitch preparation and its properties

By separating the aromatic compounds in the pyrolytic oil's heavy phase (*HS*$_{@400°C}$) structure by the vacuum distillation process carried out at 250 °C at 50 mbar vacuum pressure for 24 h with a yield of 17.02 %, biopitch *(HS-P50-250°C-24h)* to be employed as a precursor in the formation of carbon foam was achieved. Several techniques were used to clarify the biopitch's structure, including elemental analysis (C% = 73.93 %, Leco CNH628 S628), helium gas pycnometer (ρ_{true} = 1.19 g/cm^3, Micromeritics, Accupyc II 1340), thermogravimetric analysis (Setaram Labsys Evo), and Fourier transform infrared spectroscopy (PerkinElmer Spectrum 100). Ash content (*AC%* = 0.104 %, ASTM D 2415) and softening point (*SP* = 125.2 °C, Mettler Toledo FP90-83 HT) were also assessed. The biopitch's C content was about 61 % higher than that of the sawdust, and its H/C and O/C ratios were calculated to be 1.13 and 0.19, respectively. The H/C and O/C values of coal tar pitch were 0.008 and 0.0006, respectively, and those of petroleum pitch were 0.004 and 0.0008 [56,57]. This demonstrated that, in contrast to fossil pitches, the hornbeam sawdust tar pitch contains highly oxygenated and aliphatic carbons [58]. The softening point of *HS-P50-250°C-24h* coded biopitch was compatible with the softening point values (in the range of 103–129.8 °C) of biomass-based pitches in the literature [32,59–62]. Specifically, toluene and quinoline insoluble contents (*TI* and *QI*) are calculated to determine the solubility of fossil pitches. However, it was claimed that acetone was preferable for the wood tar pitches analysis because they were mainly soluble in these solvents. The acetone-insoluble fraction (*AI%*), a factor corresponding to the polymerization degree for wood tar pitches, was 32.3 %. The polymerization degree of pitches with elevated softening points was reported to rise as the relationship between SP and AI% was implied to be direct [63]. The FT-IR spectrum of the biopitch, which had a complex composition and contained lignin-derived compounds [58], was investigated. Aliphatic (CH stretching vibrations ~2900 cm^{-1}, C≡CH alkyne stretching vibrations at 2100 cm^{-1}) and aromatic (C=C$_{ar}$ stretching band between 1600 and 1400 cm^{-1}, CH bending band of syringyl and guaiacyl units at 1115 cm^{-1}, C=C cis-bending band at 750 cm^{-1}) hydrocarbons, free alcohol and phenols (3600–3200 cm^{-1} for –OH and –COOH), ethers, esters and ketones (~1700 cm^{-1} for unconjugated C=O tensile vibration) characteristic absorption bands for the structure of the pitch were observed. The presence of hydroxyl and carboxyl groups in the biopitch, which was determined to have an O content of 18.30 % calculated from the elemental analysis, was supported [56,57,64,65]. Thermogravimetric analysis was used to examine the behavior of the biopitch in the high-pressure/temperature reactor against the heating procedure applied during the foaming process. The temperature profile indicated that the decomposition reactions began at 200 °C and continued up to 620 °C. It was found that the biopitch formed around 44 % residue at 450 °C and decomposed at a rate of 63 % at 620 °C due to the oxygen in the structure enabling the biopitch's self-combustion during the foaming process.

2.4. Synthesis and characterization of hard template SBA-15

4 g non-ionic copolymer surfactant (Pluronic P123; average MW 5800, Sigma-Aldrich) was dissolved in 125 mL deionized water and 20.59 mL HCl. After dissolution was completed, dropwise additions of 9.04 mL of TEOS (tetraethylorthosilicate, Sigma-Aldrich) were applied to the solution. The synthesis solution was agitated for 24 h at 35 °C and then poured into a Teflon autoclave for hydrothermal treatment (24 h at 120 °C). The solid matter was separated, rinsed with deionized water, and dried at 65 °C for 24 h. The final solid was calcined at 550 °C for 5 h in dry air [66,67]. The organic template (P123) is entirely removed during the calcination process, which also condenses silanol groups and enables comparison of SBA-15's distinctive characteristics. Nitrogen adsorption-desorption (BET, Quantachrome Quadrosorb SI), x-ray diffraction (XRD, PANalytical Empyrean, in the range of 2θ = 0–10°), scanning electron microscopy (SEM, Zeiss Supra VP 40) analyzes were used in the characterization of support material SBA-15. The sample was pretreated at 300 °C for 5 h prior to BET analysis to remove moisture in the structure.

The morphology and surface topology of SBA-15 used as hard template material in carbon foam production were determined by examining SEM images. As seen from Fig. 1a, it was determined that the SBA-15 material had a distinct and uniform short rod-like spherical structure, the width of the formed rods was around ~0.7 μm and the length was between around 0.8 and 1.4 μm. It is known that the rod-shaped

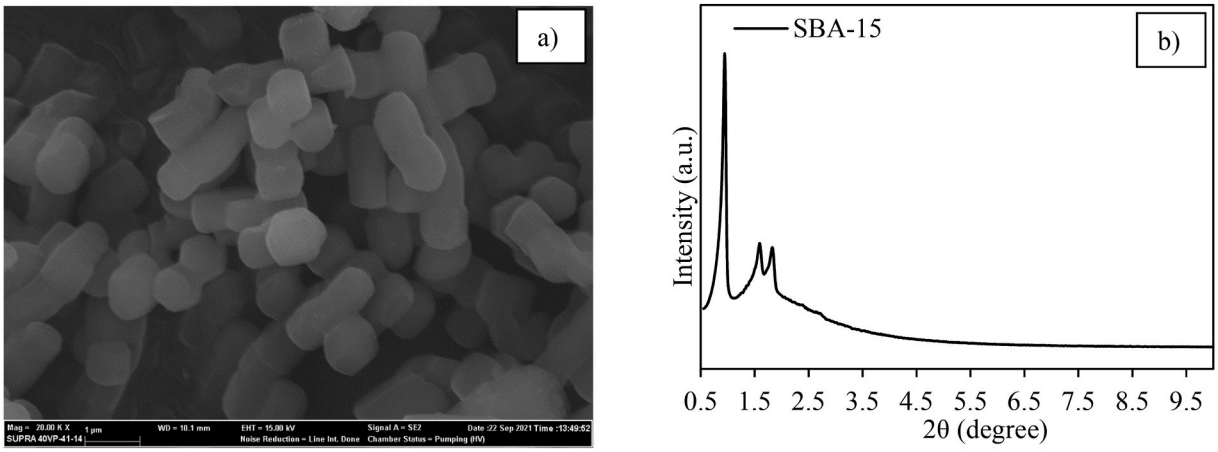

Fig. 1. (a) SEM image (20Kx) and (b) XRD pattern of the SBA-15 hard template.

morphology arises due to the static conditions used during SBA-15 template synthesis, and the formation of a high specific surface area is supported as a result of the well-organized morphology of the material [68]. The surface area of SBA-15 was determined as 786.11 m^2/g according to multi-point BET analysis and the XRD pattern of SBA-15 was given in Fig. 1b. The peaks observed at 2θ values of 0.91°, 1.58°, and 1.83° corresponded to (1 0 0), (1 1 0), and (2 0 0) reflections of characteristic regular hexagonal mesostructures [69–71]. The sharp (1 0 0) peak exhibited by the SBA-15 template in the low-angle range showed that the sample had periodic structures [69].

2.5. Preparation and characterization of HS pitch-based carbon foams

2.5.1. Green foam production without template

The as-synthesized green foam (*HSPCF*) was produced in a Parr reactor (4575B, Parr Instrument Company, USA) by the foaming process of hornbeam sawdust biopitch. The reactor was fed with nitrogen to an initial reactor pressure of 1 MPa, then heated to a target temperature (450 °C) at a heating rate of 2.5 °C/min, and eventually remained at the final temperature for 1h. The green pitch foams were eventually obtained by releasing the reactor pressure to atmospheric pressure and allowing it to cool down to ambient temperature. The volatiles formed from the light fractions and components degraded by heat treatment act as "bubble agents" during the heating of the pitch and expand the volume of the foaming precursor. The pitch molecules are oriented parallel to the bubble surface due to shear stress caused by the bubbles growing under pressure. Raising the temperature causes the biopitch to solidify, which fixes the foam matrix [72]. When the pitch undergoes a reduction of the stress arising from the pressure, its cells begin to expand and volatiles are released [73]. The carbon foam production yield from hornbeam sawdust biopitch was computed as ~41.56 %.

2.5.2. Green foam production with hard template SBA-15

To obtain foam utilizing a hard template, foaming at 450 °C in the high temperature/pressure reactor after mixing a certain amount of SBA-15 and biopitch according to the template ratio to be applied, and carbonization at 1050 °C was carried out. The samples were kept in 2 M NaOH solution for 150 min, then filtered, washed until the pH was neutral, and dried at 100 °C to dissolve the SBA-15 templates in the structure of the carbonized foams and remove them from the foam cage [74]. The treatment process with sodium hydroxide, which was carried out to remove the silicon atoms in the SBA-15 structure, is defined as anisotropic wet etching. Pure inorganic aqueous solutions of potassium hydroxide and sodium hydroxide have long been known to anisotropically etch the silicon. In addition, it is known that all aqueous solutions containing other alkali metal hydroxides such as ethylenediamine pyrocatechol (EDP), hydrazine (N_2H_4-H_2O) and LiOH or CsOH are used as abrasives in the anisotropic etching process [75]. On the other hand, it is known that the use of HF, HF:NH_4F, and HF:HNO_3:CH_3COOH:H_2O, which are among the isotropic etchants, has environmental disadvantages [76]. The hydroxide etching reaction of silicon was viewed in Eqs. (1)–(3), and the overall redox reaction was given in Eq. (4). According to the reaction mechanism, in the first step, silicate formation occurred as a result of silicon oxidation by hydroxyl ions (Eq. (1)), and in the second step, after water was reduced (Eq. (2)), silicate ions reacted with hydroxyls to form a water-soluble complex (Eq. (3)) [75,77–79].

$$Si + 2OH^- \rightarrow Si(OH)_2^{2+} + 4e^- \quad (1)$$

$$4H_2O + 4e^- \rightarrow 4OH^- + 2H_{2\,(gas)} \quad (2)$$

$$Si(OH)_2^{2+} + 4OH^- \rightarrow SiO_2(OH)_2^{2-} + 2H_2O \quad (3)$$

$$Overall\ reaction: Si + 2OH^- + 2H_2O \rightarrow SiO_2(OH)_2^{2-} + 2H_{2\,(gas)} \quad (4)$$

The carbon atoms in the foam structure reacted with sodium hydroxide, which broke the C–O–C and C–C bonds in the structure, in addition to elimination and dehydration reactions, according to the activation mechanism given in Eq. (5) [80–82].

$$6NaOH + 2C \leftrightarrow 2Na + 2Na_2CO_3 + 3H_2 \quad (5)$$

2.5.3. Chemical activation and carbonization procedures

To improve the surface area of the as-synthesized green foam obtained by the traditional foaming method, chemical activation with potassium hydroxide (KOH) at a foam:activation agent mixture ratio of 1:1 (w/w) was adopted [83]. In the as-synthesized green foams produced with the template technique, after the SBA-15 template was removed from the structure, the activation step with KOH was performed. In the last step, the as-synthesized green foam and activated foam were treated with N_2 (flow rate 100 mL/min) at 1050 °C with a heating rate of 5 °C/min and carbonized for 2 h. Then, carbon foam production was completed by washing the samples with distilled water till the acidity level was neutral to remove K^+ ions from the structure and finally dried at 110 °C in an oven. During the carbonization process, the foam was prevented from splitting at high temperatures, and the volatile substances were also removed by the nitrogen gas fed into the system. After being prepared without using a template, the carbonized foams were coded according to whether they were synthesized from hornbeam sawdust-based biopitch (*HSPCF*) or chemically activated with KOH (*HSPACF*). Carbon foams prepared using a hard template were coded as *HSP-S-x* or *HSPA-S-x* depending on their activation status. Here, the term "*x*" represents the ratio of the SBA-15 template added by weight 1, 5, 10, 20, and 30 %.

The chemical reactions that occurred during the heat treatment process of increasing the surface area using potassium hydroxide were given in detail [32]. When potassium hydroxide was used; the reaction between the carbon in the foam matrix and the activation agent occurred as a solid-solid phase reaction and continued as a solid-liquid reaction. In this scenario, the potassium species was reduced to generate K metal, carbon was oxidized to carbon oxides and carbonates, and further reactions took place between several active intermediates [84]. Potassium carbonate (K_2CO_3) and potassium hydroxide (KOH) reacted with the carbon to get metallic potassium. In addition, carbon monoxide gas was produced by the decomposition of K_2CO_3, and the resulting gas acted as a secondary activation agent through depolymerization reactions. The redox reaction between KOH and carbon, and even additional potential reactions were given in Eqs. (6)–(14) [85,86]. As reported in the research to date, the reactions that take place when different carbon sources are activated with KOH primarily rely on three mechanisms: *i)* chemical activation (Eqs. (6), (9) and (11)); *ii)* physical activation (Eqs. (7), (8) and (10), (12)–(14); and *iii)* incorporation of metallic K into the carbon matrix and development of the carbon lattices [32,84,86].

$$6KOH + 2C \rightarrow 2K + 3H_2 + 2K_2CO_3 \quad (6)$$

$$2KOH \rightarrow K_2O + H_2O \quad (7)$$

$$K_2CO_3 \rightarrow K_2O + CO_2 \quad (8)$$

$$K_2CO_3 + 2C \leftrightarrow 2K + 3CO \quad (9)$$

$$K_2O + H_2 \rightarrow 2K + H_2O \quad (10)$$

$$K_2O + C \rightarrow 2K + CO \quad (11)$$

$$C + H_2O \rightarrow CO + H_2 \quad (12)$$

$$CO + H_2O \rightarrow CO_2 + H_2 \quad (13)$$

$$CO_2 + C \rightarrow 2CO \quad (14)$$

2.5.4. Characterization of carbon foams

Elemental analysis (Leco CNH628 S628), which detects the CHN content, was initially applied to clarify the foams' characteristics. The scanning electron microscope (Zeiss Supra VP 40) images with platinum sputter-coated (Quorum Q 150 R ES DC Sputter) were used to identify the surface morphologies of the foams. PANalytical Empyrean x-ray diffraction instrument with CuKα radiation (λ = 0.15406 nm) was employed to ascertain the crystalline forms and compute the interplanar spacing (d-spacing) in the atomic lattice in the 2θ range of 0° and 80°. Nitrogen adsorption/desorption isotherms of the foams were obtained at 77 K after degassing at 300 °C in a nitrogen atmosphere for 6 h, pore volumes and surface areas (S_{BET}) were computed via the Brunauer Emmett and Teller method employing the Micromeritics ASAP 2020 gas adsorption analyzer. The pore size distributions of foams produced without applying the template technique were determined in conformity with the density functional theory (DFT). Furthermore, compressive strength tests were undertaken on a Shimadzu AG-IC 100 KN tensile/compression device with a loading rate of 0.5 mm/min, and the Renishaw Raman inVia microscope was used to record confocal Raman spectra. The carbon foam's bulk density was estimated by weighing foam with certain dimensions, and true density was identified with a helium gas pycnometer (Micromeritics, Accupyc II 1340), and the porosity(%) values were computed through Eq. (15). The porosity(%) and the theoretical and actual volumes of foams were symbolized as P, V_t, and V_a in Eq. (15) [87].

$$P = (V_t - V_a) / V_t \quad (15)$$

Based on the crystal structure, surface area, and compressive strength values, the textural analysis of the foams formed according to optimal experimental parameters was examined with a transmission electron microscope (TEM, JEOL 1220 JEM, 80 keV) images and thermal conductivity measurements (C-Therm TCI 2A) were performed at ambient temperature.

3. Results and discussion

3.1. Elemental analysis

The variations in C(%), H/C, and O/C values of the *HS*-based foams according to the elemental analysis were compared concerning the template proportion and chemical activation treatment, and the data were presented in Table 1. The carbon levels of the foams were significantly higher (between 86.63 and 60.76 %) than those of the sawdust (45.99 % C) and pyrolytic oil (59.94 % C), confirming that biopitch-based foams were more enriched in carbon than *HS*. While the elemental C content of the carbon foam formed without the template technique was 86.63 %, the C content decreased by 5 %–82.27 % after chemical activation treatment. Given that biopitch had a C content of 73.33 % and an O content of 18.30 %, it was established that the C content of *CFs* was greater than that of biopitch, and the O content was inversely proportionally smaller (10.81 % and 15.46 % for *HSPCF* and *HSPACF*, respectively).

A mixture of biopitch and oxygen-containing SBA-15 (with the empirical formula of SiO_2) was placed in the molds in the reactor where foaming occurred when the template technique was implemented. The number of oxygenated groups provided to the synthesis medium increased as the template ratio raised from 1 % to 30 % in the carbon foam development technique employing a hard-silica template. Shim et al. [88] showed that when pitch-based carbon fibers were treated with NaOH under mild temperatures to provide oxidation of the carbon material surface, the physicochemical properties of the active fibers could be modified. Tseng [89] verified that elemental analysis revealed a drop in nitrogen content and an increase in oxygen content in the activated carbon resulting from the char treatment with NaOH. Since the carbon skeleton was also impacted by the NaOH etching process used in this study to produce biopitch-based carbon foam via the SBA-15 template, the carbon foam's surface was altered due to oxidation, its functionality changed, its oxygen content rose, and its nitrogen content fell—all of which were in line with the previously mentioned studies. The amount of elemental C in the structure of carbon foams was determined to be reduced because the oxygenated species enable self-combustion during the heat treatment used in the foaming and carbonization stages. Furthermore, the C ratio in the activated carbon foam structure was diminished as a consequence of the carbon in the

Table 1
Elemental analysis of *CFs* produced at 1 MPa and 450 °C.

Foam code	C (%)	H (%)	O (%)	N (%)	HHV (MJ/kg)	H/C	O/C
Produced by conventional method without a template							
HSPCF	86.63	0.59	10.81	1.97	28.20	0.08	0.09
HSPACF	82.27	0.82	15.46	1.45	26.21	0.12	0.14
Produced by a hard template-assisted method							
HSP-S-1	85.85	0.58	12.46	1.12	27.62	0.08	0.11
HSP-S-5	79.69	0.60	18.75	0.96	24.43	0.09	0.18
HSP-S-10	77.88	0.81	20.39	0.93	23.83	0.12	0.20
HSP-S-20	70.03	0.80	28.36	0.81	19.73	0.14	0.30
HSP-S-30	67.32	1.66	30.74	0.29	19.61	0.30	0.34
HSPA-S-1	79.83	1.15	17.86	1.16	25.44	0.17	0.17
HSPA-S-5	73.73	0.78	24.76	0.74	21.59	0.13	0.25
HSPA-S-10	73.61	0.95	24.86	0.59	21.78	0.15	0.25
HSPA-S-20	68.62	1.37	29.36	0.65	19.88	0.24	0.32
HSPA-S-30	60.76	0.79	37.66	0.79	14.89	0.16	0.46

foam structure reacting with the activation agent during potassium hydroxide activation. Although the O/C ratio of carbon foam produced without a template was 0.09, the ratio of carbon foam with SBA-15 additive varied between 0.11 and 0.34. The O/C ratios of hard-silica template-added activated carbon foams were identified to be between 0.17 and 0.32. In the present scenario, applying the activation technique after the foaming stage resulted in activated foams with lower C and higher O contents than non-activated carbon foams.

3.2. Textural analysis

Carbon foam is described as a carbon framework with specific amounts of cells, and foam cell shape has a substantial impact on carbon foam strength. The micro- and mesopore morphology of the foam framework, on the other hand, influences the strength of carbon foam [90]. Surface area and pore properties, which were notable parameters for porous materials, were examined using nitrogen-sorption analysis. The pore volume, surface area, and average pore diameter values of the carbon foams produced without using the template technique were determined by the Density-Functional Theory (DFT) method and presented in Table 2, the pore size distribution graphs and nitrogen adsorption/desorption isotherms were given in Fig. 2. The rise in adsorbed volume at a relative pressure of $P/P_0 < 0.1$ revealed the existence of micropores in carbon foams by the isotherm behavior. Additionally, the growth in adsorbed volume in the region right after $P/P_0 > 0.9$ suggested the existence of macropores, and the increase between $P/P_0 = 0.01$ and $P/P_0 = 0.30$ demonstrated a normal distribution of mesopores in the structures. The hysteresis arising in the adsorption and desorption isotherms generally implied that the pore shapes in the carbon foams were not homogenous [16]. The surface area of *HSPCF* carbon foam, which had a low value (59.8 m^2/g), increased to 1004.2 m^2/g for *HSPACF* due to the cracks and smaller pores formed in the structure after chemical activation as supported by SEM analysis. This situation was compatible with the pore volume in the structure, which was 0.037 cm^3/g for *HSPCF* and increased to 0.423 cm^3/g in activated carbon foam *HSPACF*. Porous solid materials are classified considering pore sizes according to IUPAC as *i)* microporous if the pore diameter is less than 2 nm, *ii)* mesoporous if the pore diameter is in the range of 2–50 nm, *iii)* macroporous if the pore diameter is greater than 50 nm [91]. In the nitrogen-sorption isotherms of carbon foams, a trend towards type IV isotherm, which indicated the presence of meso and micropores according to the IUPAC classification, was observed, and the mean pore diameter (D_{av}, nm) values of both foams were found to be 1.22 nm. According to the pore size distribution graphs, it was determined that the pore size distribution of the activated carbon foam was more homogeneous than the non-activated carbon foam.

Adsorption isotherms in the range of $P/P_0 = 0–0.4$, used in the calculation of the multi-point BET (Brunauer-Emmett-Teller theory) surface area of carbon foams produced by the template method, were given in Fig. 2b and c. According to the multi-point BET surface area values of carbon foams (Table 3), it was determined that the surface area reached 569.3 m^2/g without chemical activation by using SBA-15 material as a template at 30 wt% ratio. A significant increase in surface area was observed as a result of the hard template removal from the structure and the formation of related pores in the carbon foam structure. Carbon foams synthesized using SBA-15 were treated with NaOH to remove silica in the structure. During this process, keeping the carbon foam in NaOH solution both removed the silica from the structure and led to the formation of smaller pores due to the chemical activation caused by the reaction between carbon and a strong base. Dehkordi et al. [92] modified commercial activated carbon at room temperature using different concentrations of NaOH (0.01–8 M). As a result, they confirmed the validity of the reaction mechanism between sodium hydroxide and C element in the activated carbon structure given in Eq. (5) based on the decrease in elemental C content of the activated carbon, as well as changes in SEM images, BET surface areas, and Raman spectra. Thus, the surface area value enlarged from 4.0 m^2/g to 569.3 m^2/g when the SBA-15 ratio was increased from 1 % to 30 % by weight. When the surface areas of activated carbon foams were compared, it was given that the surface area increased proportionally with the rising amount of template (SBA-15). It was clearly seen from the SEM images (Figs. 4 and 5) that when the SBA-15 template addition was at 10 wt% and over, the carbon skeleton that forms the carbon foam structure turned into a form containing smaller pores instead of a reticular structure. As a result of the interaction between carbon foams and potassium hydroxide, many smaller pores were formed within the macropores of carbon materials.

Table 2
Textural properties of *CFs* prepared without using templates.

Foam code	Surface Area (m^2/g)	V_{total} (cm^3/g)	V_{micro} (cm^3/g)	V_{meso} (cm^3/g)	D_{av} (nm)
HSPCF	59.8	0.037	0.018	0.019	1.22
HSPACF	1004.2	0.423	0.392	0.031	1.22

3.3. XRD analysis

In the x-ray diffraction patterns of carbon foams made from hornbeam biopitch (Fig. 3), a broad band of stacked graphitic basal plane (0 0 2) associated with carbon-based materials emerged between $2\theta = 10°$ and 30°, with its highest value being close to $2\theta = 23°$ [32,85,93–96]. The (0 0 2) peak arose at elevated temperatures near 1400–1500 °C in similarly structured substances comprising eucalyptus lignin and reinforced phenol-formaldehyde resin-based fibers. The thermoplastic features of biopitch and the existence of low-molar weight molecules could be relevant for the (0 0 2) peak's development at a moderate carbonization temperature (1050 °C). Both of these features improved the structural arrangement during the initial heating stage, which aided in the growth of carbon crystals [62]. It was likewise acknowledged that the ordinary reflection of the two-dimensional arrangement of carbon layers in graphite-like matters had the planes of (1 0 0) and (1 0 1) between $2\theta = 41°$ and 45° [97,98]. This reflection signed that aromatic rings began to condense and form two-dimensional clusters at an operational temperature of 1050 °C [62].

The hexagonal carbon (0 0 2) and hexagonal graphite (1 0 0) planes of arbitrarily stacked graphene sheets, respectively, were recognized by the diffraction peaks in the XRD profiles near $2\theta = 23°$ and 43° [52,84,99–101], while the orthorhombic graphite was marked by the peak at $2\theta = 72°$ [102]. Carbon foams with identical x-ray diffraction patterns suffered chemical activation, which resulted in a reduction in the intensity of reflections of the (0 0 2) and (1 0 0) planes. The raised reflection intensity of these two planes in the x-ray diffraction patterns of carbon/activated foams generated with the incorporation of 1 wt% SBA-15 template suggested that the crystalline structures of the mentioned foams were more developed. The reflection intensities of the (0 0 2) and (1 0 0) planes of the templated with 30 wt% SBA-15 and activated foam (*HSPA-S-30*) were the lowest peaks within all patterns.

3.4. Scanning and transmission electron microscopy image analyses

Two unique pores are identified by the terms utilized to describe carbon foams: i) *cell*: a macropore surrounded by a carbon wall; ii) *window:* a hole created in the carbon wall that allows neighboring cells to connect. In the carbon cell wall, micropores, mesopores, and smaller macropores than cells may appear. Carbon foam, consequently, can be described as "a material with a porous structure, in which cells are linked together via windows" [62,103]. Figs. 4 and 5 illustrated SEM images obtained to gain insight into the morphological structures of non-activated and activated carbon foams produced by biopitch foaming through conventional and template-assisted methods. At 100x magnification, the SEM images of the *HSPCF* and *HSPACF* foams shown in Fig. 4 indicated that both carbon foams had porous structures. When the

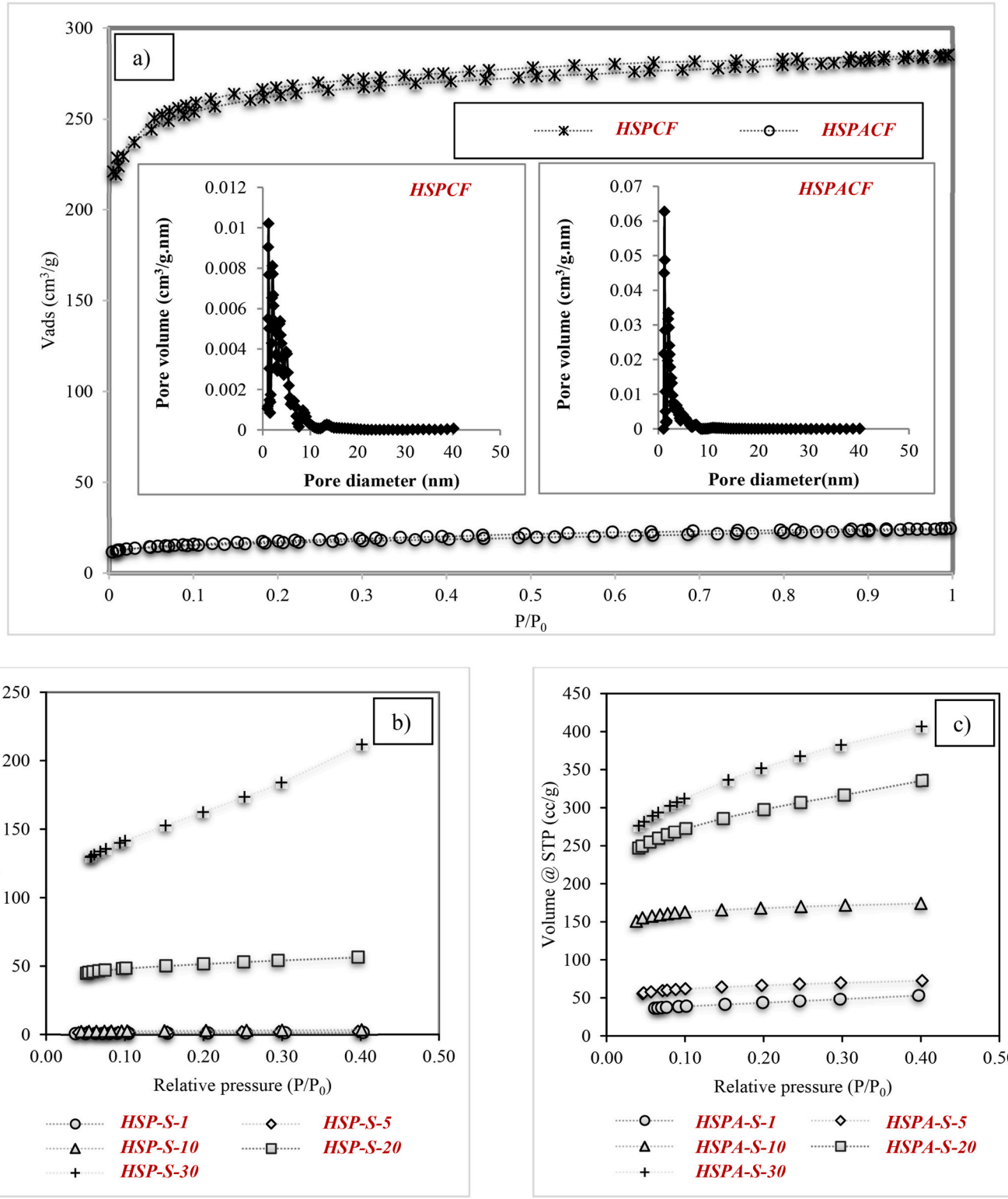

Fig. 2. (a) Nitrogen adsorption/desorption isotherms and DFT pore size distribution graphs for carbon foams produced without using templates, (b) and (c) adsorption isotherms ($0 < P/P_0 < 0.4$) of carbon foams produced via template-assisted method.

HSPCF carbon foam was activated with KOH, it became clear that in addition to breaks in the nodal points and cell walls of the *HSPACF* foam, micro-cracks appeared in the structure. This structural modification improved surface area while reducing compressive strength. The existence of cells ranging in size from 50 to 400 μm was noticed in the carbonized and activated foam structures' that were generated without the template technique. Fig. 5 showed SEM images of foams created using SBA-15 as a hard-silica template. When the chemical activation technique was performed on carbon foams produced with SBA-15, fractures in the structure were detected, comparable to the morphology of activated foam prepared without the template. The carbon foam (*HSP-S-1*) formed when 1 % by weight of SBA-15 was

Table 3
S_{BET} of carbon/activated foams prepared via template-assisted method.

Carbon foam code	Surface Area (m^2/g)	Activated foam code	Surface Area (m^2/g)
HSP-S-1	4.0	***HSPA-S-1***	151.5
HSP-S-5	6.3	***HSPA-S-5***	242.1
HSP-S-10	9.7	***HSPA-S-10***	648.3
HSP-S-20	191.9	***HSPA-S-20***	1073.0
HSP-S-30	569.3	***HSPA-S-30***	1226.9

utilized as the template shown in Fig. 5a contained cells ranging in size from 480 to 975 μm and voids ranging from 235 to 785 μm. Fig. 5b demonstrated that the cell sizes of the activated foam (*HSPA-S-1*) varied between 500 and 940 μm, and the size of the voids changed between 100 and 515 μm. The carbon foam (*HSP-S-5*) formed by increasing the SBA-15 template ratio from 1 % to 5 % by weight displayed a morphology with larger cell sizes between 450 and 1400 μm. However, the void sizes of *HSP-S-5* (85–415 μm) altered between 170 and 525 μm as a result of chemical activation (*HSPA-S-5*) (Fig. 5c and d). Furthermore, it came to light that the formation of tiny voids initiated on the surface. The size of the holes varied in inverse relation to the quantity of hard-template comprised. While the SBA-15 ratio was 10 wt%, no distinguishable cell frameworks formed in the *HSP-S-10* carbon foam, as well as numerous microvoids and inhomogeneous voids in the 45–235 μm size range appeared (Fig. 5e). On the other hand, the porosity of the activated foam *HSPA-S-10* increased via the activation process. When the SBA-15 ratio was increased to 20 % and 30 % by weight, as shown in Fig. 5g–j, cells that should be present in the carbon foam skeleton did not

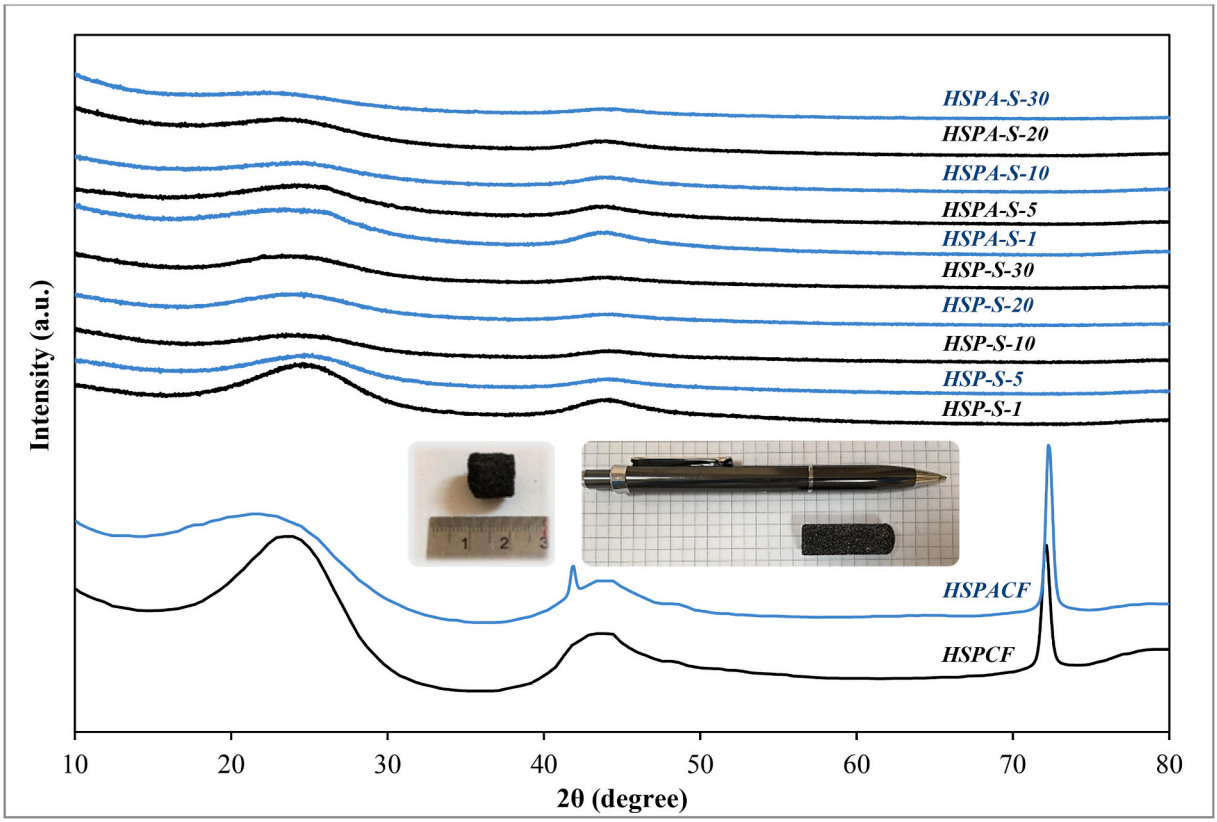

Fig. 3. XRD patterns of carbon/activated foams prepared by conventional method without a template and hard template-assisted method.

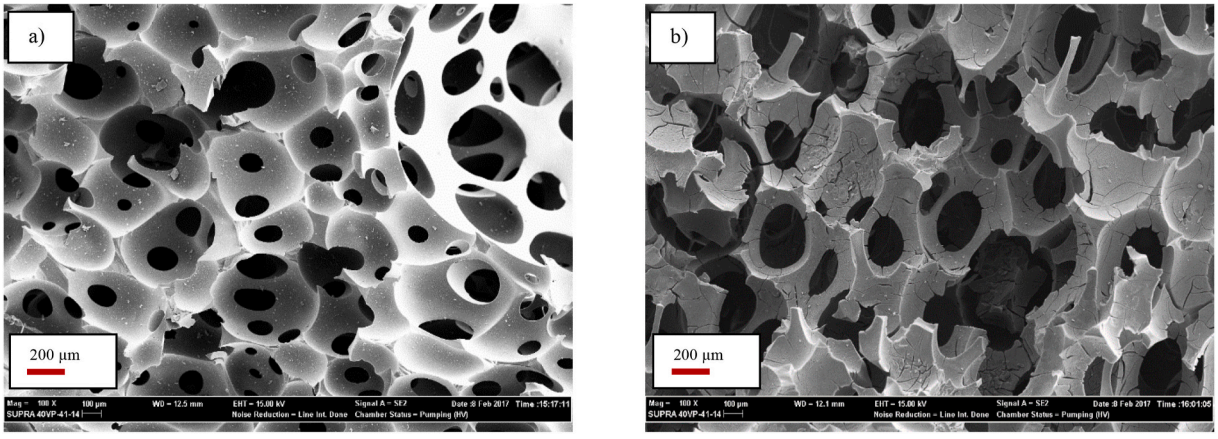

Fig. 4. SEM images of (a) *HSPCF* and (b) *HSPACF*.

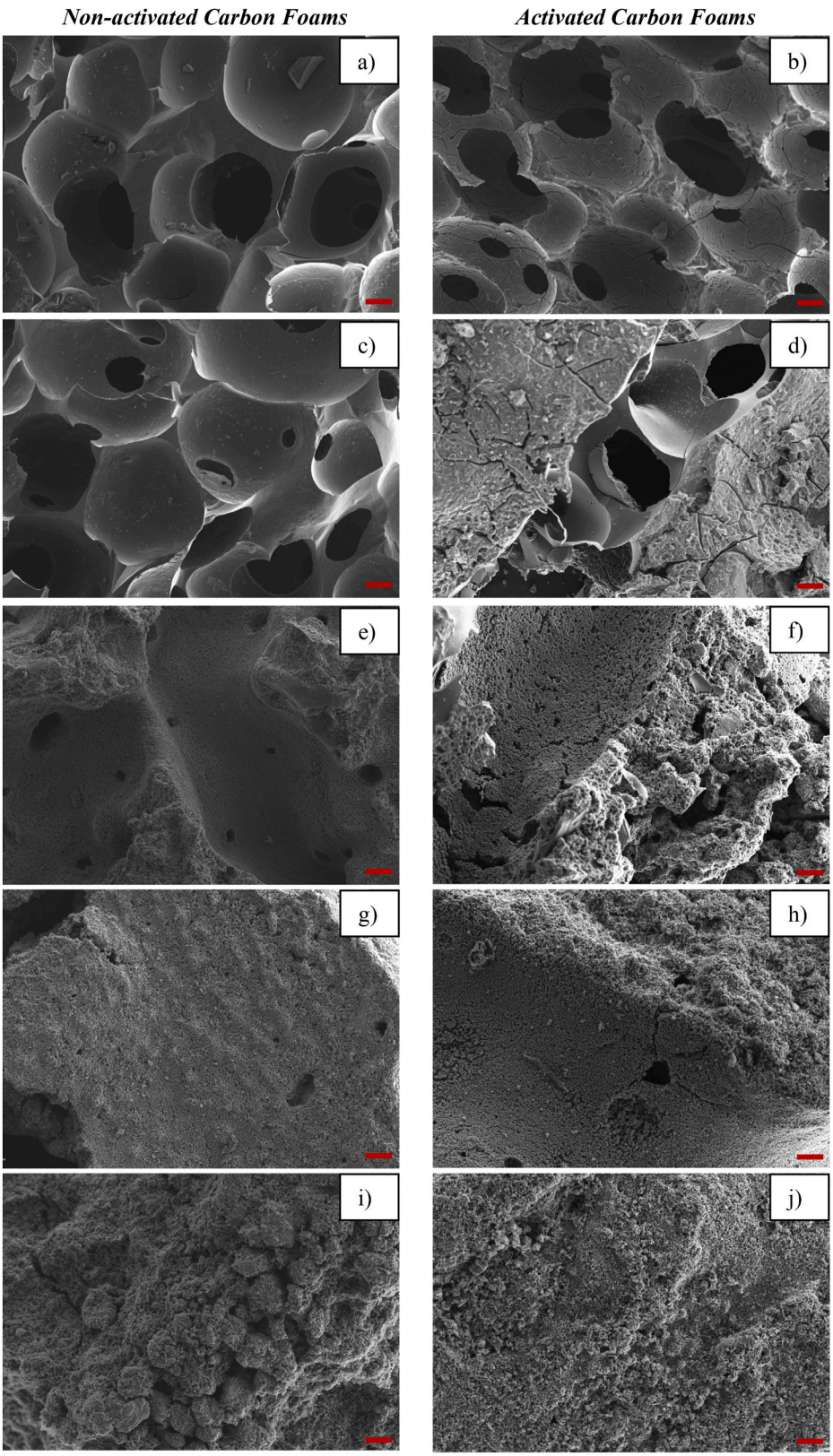

Fig. 5. SEM images (100x) of (a) *HSP-S-1*, (b) *HSPA-S-1*, (c) *HSP-S-5*, (d) *HSPA-S-5*, (e) *HSP-S-10*, (f) *HSPA-S-10*, (g) *HSP-S-20*, (h) *HSPA-S-20*, (i) *HSP-S-30,* and (j) *HSPA-S-30* (scale 200 μm).

form, and numerous microscopic voids were detected in both the carbonized and activated foam structures. It was substantial that the carbon foams had amorphous porous networks and the existence of graphitic carbon areas developed due to the overlap of graphene layers in all carbon foams, as shown by the TEM images (Fig. 6) assessed for the elucidation of the textural characteristics. In accordance with the XRD patterns, a portion of the amorphous carbon derived from the bio-pitch had converted into crystalline graphite, which probably caused the shift

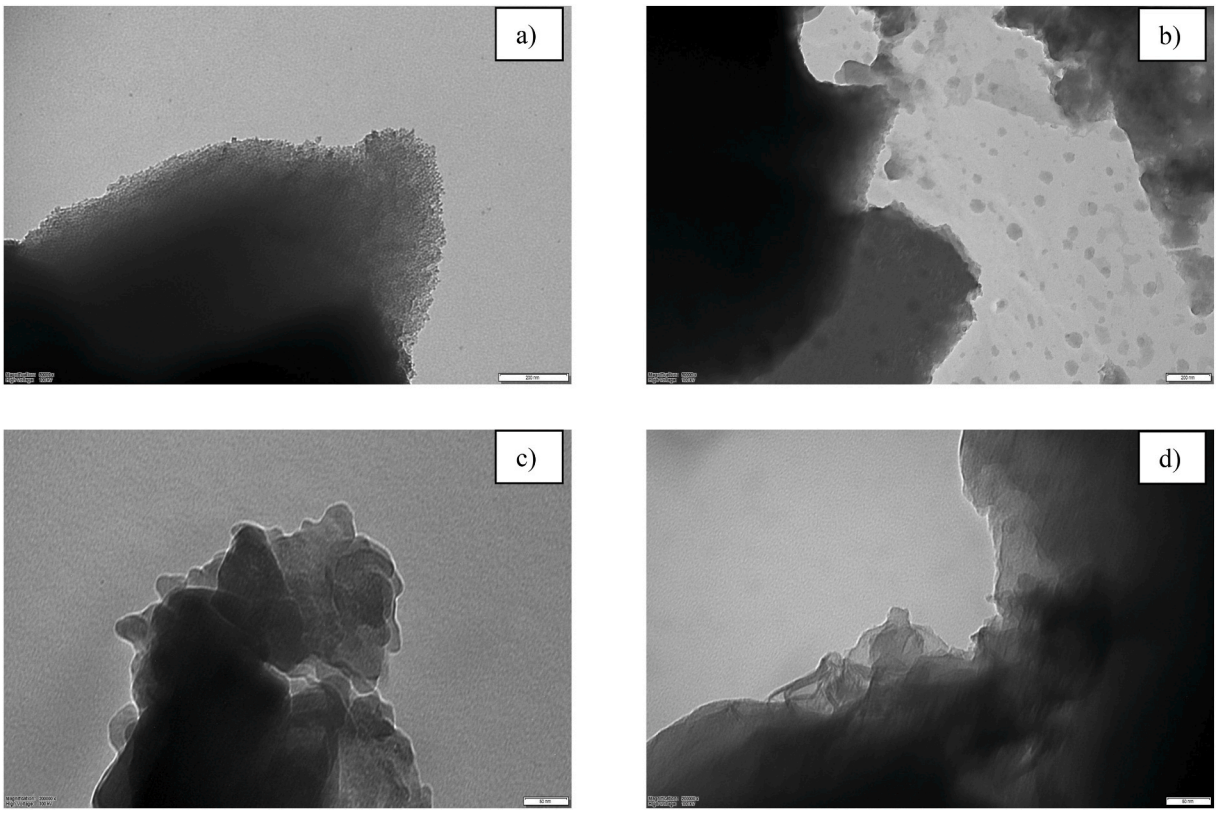

Fig. 6. TEM images of (a) *HSPCF*, (b) *HSPACF*, (c) *HSP-S-1*, and (d) *HSPA-S-1*.

to the right of the ordinary peak (0 0 2) occurring at ~23° for graphite upon chemical activation.

3.5. Porosity analysis, measurements of compressive strength, and thermal conductivity

The density of closed-cell foams is well-known to be the primary factor influencing their mechanical characteristics and thermal conductivity [102]. Table 4 presented the measurement results of the compressive strength values associated with the carbon foams' densities and pore structures. The decrease in compressive strength values with the improvement in porosity and pore volume coincided with the studies carried out in the literature [32,102]. The bulk density and porosity(%) values calculated based on the true density measured with a helium pycnometer revealed that the porosity of the *HSPACF* carbon foam formed through chemical activation was 4.2 % higher than that of the *HSPCF*. In comparison to *HSPCF* carbon foam, hard template-produced carbon foams were shown to have greater bulk and true density values. Foams' bulk densities range from 0.15 to 0.43 g/cm^3, while their true densities vary between 1.64 and 1.99 g/cm^3. It was determined that the foams' true density increased while their bulk density diminished after the potassium hydroxide activation process. As a result of the activation procedure, a rise in porosity values was noted. The compressive strength test revealed that after chemical activation, the 1.681 MPa *HSPCF* carbon foam's compressive strength value dropped to 0.258 MPa. It was found that the compressive strength of carbon foams ranged from 1.681 to 7.146 MPa, whereas the values for activated foam varied between 0.258 and 0.723 MPa. Scanning electron microscopy and surface area investigations ascertained that porosity increased due to the activation treatment. It was noted that the compressive strength of foams reduces as their structure becomes more porous. According to Chen et al. [90], foam with a thicker cell wall and a smaller cell

Table 4
Carbon foams' compressive strength, density, and porosity(%).

Foam code	Compressive strength (MPa)	Bulk density (g/cm^3)	True density (g/cm^3)	Porosity (%)
Produced without applying the template technique				
HSPCF	1.681	0.19	1.64	88.55
HSPACF	0.258	0.16	1.99	92.24
Produced using a hard-silica template				
HSP-S-1	7.146	0.43	1.76	75.28
HSP-S-5	3.158	0.43	1.72	74.79
HSP-S-10	1.464	0.43	1.73	74.96
HSP-S-20	0.696	0.36	1.83	80.49
HSP-S-30	–	–	1.71	–
HSPA-S-1	0.723	0.40	1.80	77.93
HSPA-S-5	0.509	0.38	1.82	79.36
HSPA-S-10	0.368	0.36	1.82	80.07
HSPA-S-20	0.258	0.19	1.89	89.99
HSPA-S-30	–	–	4.13	–

cross-section had greater compressive strength. A denser arrangement was formed as a consequence of improved cross-linking and aromaticity of the molecules, which was reflected in a rise in the actual density as determined by the helium pycnometer. Furthermore, the generation of planar aromatic ring clusters at high temperatures was also known to result in heavier structures than disordered carbons and increasing density [97].

To sum up, this research was offered to increase porosity with chemical activation and thus develop carbon foams with large surface areas, even if their compressive strength is low, for use as an adsorbent and catalyst support. After the template approach, the goal was to use the etching procedure to eliminate SBA-15. The foam produced in the high-temperature/pressure reactor had a very dense and rigid structure. Accordingly, it could be concluded that SBA-15 particles settled in the foam pores could be partially removed since NaOH penetration to the inner parts of the SBA-15/carbon foam composite structure may have been limited during the etching process. Therefore, when only carbonization was applied to the samples to which SBA-15 was added up to 10 % by weight, the lower surface areas were a result of the blocking of the pores in the carbon skeleton and the inability to adsorb N_2 gas in the pores of the deepest part. These data were compatible with the high compressive strength and bulk density. When the loading ratio exceeded 20 % by weight, more porosity was formed after the silica on the surface of the carbon foam was removed or the activation process was involved after the template technique; accordingly, the surface area increased and the strength of the carbon network decreased.

Foams derived from natural resources are cheap and easy to produce. In contrast to graphitic foams, which typically have a thermal conductivity of 100–200 W/m.K [11], they have inferior thermal conductivity (<0.2 W/m.K). The material's thermal conductivity becomes crucial depending on the area of application. The literature mentioned that phenolic-based foams possessed thermal conductivities that ranged from 0.06 to 0.24 W/m.K [104–106]. Researchers of Oak Ridge National Laboratory (ORNL) conducted tests in which carbon foam was created without the blowing and stabilizing processes. Foams with graphitic structures were noticed to have high thermal conductivity coefficients of 180 W/m.K. These foams, known as PocoFoam™ [107,108], were the first foams in the literature to have a bulk thermal conductivity value higher than 50 W/m.K. A novel carbon foam was also created by researchers from the same company utilizing naphthalene-based mesophase pitch, which had a thermal conductivity range of 0.3–150 W/m.K [109]. Commercially available carbon foams have a wide range of thermal conductivities. For example, Ultramet's RVC foam has thermal conductivity coefficient values of 0.085 W/m.K, Touchstone foam has 0.40–17.50 W/m.K, MER foam has 0.05–210 W/m.K and ORNL foam has 0.3–180 W/m.K [62,107]. *HSPCF* and *HSP-S-1* coded foams developed within the frame of this research had thermal conductivity coefficient values of 0.056 and 0.052 W/m.K, respectively. In European standards, thermal insulation materials are those having a thermal conductivity coefficient of less than 0.065 W/m.K. It was apparent as a consequence that the foams created in this study could be regarded as thermal insulation elements.

3.6. Raman spectra analysis

Raman spectroscopy allows researchers to examine crystal structures and electrical properties of carbonaceous materials. This technique allows for the analysis of G (graphite-like), D (diamond-like), and 2D bands, along with the investigation of features comprising defects, graphene layers' number, doping level, the layers' quality, and irregular or regular structures. Specific G and 2D bands are terms used to describe the Raman bands of carbon-based materials like graphene. These bands respond quickly to variations in temperature and chemical doping. The G and 2D bands' shape, position, and intensity change as the graphene layers' number varies. Edge defects and heteroatom participation are the two kinds of defects and irregularities in the graphene crystal structure revealed by the D-band [110]. Fig. 7 presented representative Raman spectra of carbon foams, which were used to identify the carbon species in the materials. At wavelengths of 1343 cm^{-1} and 1600 cm^{-1}, respectively, characteristic peaks belonging to D-band and narrower graphite G-band types were found, confirming the formation of carbon in all materials [111]. While the G-band illustrates the formation of carbon in sp^2 regular structures, such as graphene and filament-type carbon, as a result of C-C stretching, the D-band, which corresponds to sp^3 vibrations, signifies the carbon structure irregularities, structures deformed as a result of oxidation, and defects in the graphene structure (carbonaceous materials), such as the formation of amorphous and graphite type carbon. In such a case, a lower D-band intensity in the

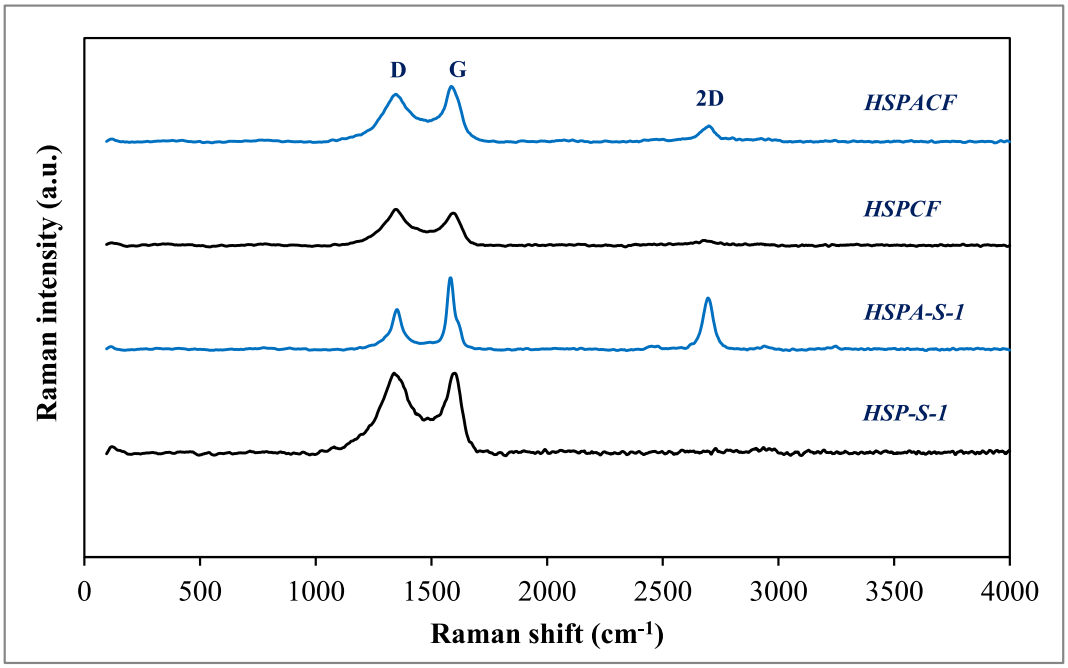

Fig. 7. Raman spectrums of carbon foams.

Raman spectrum suggested that the carbon foam's graphitization degree was greater [32,112]. The possible existence of partial lattice defects due to the number of pores in a single graphene layer was depicted by the presence of a strong D-band [32,113]. The number of layers and graphene quality influence the intensity and structure of the 2D band at ~2700 cm^{-1}. Fig. 7 showed that the band broadened due to the presence of multiple layers with some defects in the foams (*HSPA-S-1* and *HSPACF*).

4. Conclusions

Considering that pyrolysis liquid products are generally used as fuel and chemical raw material input, the evaluation of sustainable precursor materials as an alternative to mesophase pitches derived from fossil fuels in the synthesis of carbonaceous materials with tunable properties, which is becoming more crucial as technology advances, will enable the creation of a new field of usage. Within the scope of this study, it was aimed to assess industrial biomass waste hornbeam sawdust biopitch as a precursor material in the preparation of carbon foam. In this context, foaming of biopitch or biopitch-hard template (SBA-15) mixture were the two different approaches used in the foaming process carried out in the high temperature/pressure reactor. In-depth research was done on the effects of the template approach and the chemical activation procedure using potassium hydroxide on the elemental content, and crystallographic, morphological, and structural characteristics of carbon foams. It was concluded that the reduction in surface area when the hard template was applied at 1 % by weight significantly increased the compressive strength. In this case, *HSP-S-1* carbon foam with a surface area of 4.0 m^2/g had a porosity level of 75.28 % and a compressive strength value of 7.146 MPa. When the template method was implemented, the production conditions of *HSP-S-1* carbon foam were found to be ideal because this material had a more ordered crystalline structure, the level of cracks in the cells was at a minimum according to the images from the scanning electron microscope, as a result, the compressive strength value was at the highest level. The images of the multilayer graphene structure displayed by the transmission electron microscope provided evidence for the presence of pores in the foam structure. Because the produced biopitch-based carbon foams had thermal conductivity coefficient values in the 0.052–0.056 W/m.K range, it was obvious that they could potentially be employed as thermal insulation materials. The characterization procedures led to the conclusion that materials with the desired qualities may be created by altering the working conditions used during the bio-based carbon foam preparation. The ability to modify their fundamental characteristics is a significant benefit since carbon foams with hierarchically ordered pore structures and high surface areas can be employed as adsorbents, catalytic support materials, or thermal insulation materials. Regarding the product features, it is planned to investigate the properties of carbon foam utilizing several types of template materials in the foaming process within the scope of future studies. As a result, in this study, the transformation of waste disposal into sustainable production was achieved by using waste biomass in the production of technological materials.

CRediT authorship contribution statement

Adife Şeyda Yargıç: Writing – review & editing, Visualization, Project administration, Investigation, Formal analysis, Conceptualization. **Gamze Gündüz Meriç:** Writing – original draft, Investigation, Formal analysis. **Yunus Dolaş:** Formal analysis. **Nurgül Özbay:** Supervision.

Declaration of competing interest

The authors report no declarations of interest.

Acknowledgments

The authors would like to thank The Scientific and Technological Research Council of Türkiye (TÜBİTAK) under Grant Number 219M104 for financial support.

Data availability

Data will be made available on request.

References

[1] O.M. Alifanov, S.A. Budnik, A.V. Nenarokomov, M.O. Salosina, Design of thermal protection based on open cell carbon foam structure optimization, Appl. Therm. Eng. 173 (2020) 115252, https://doi.org/10.1016/j.applthermaleng.2020.115252.
[2] S. Yu, Z. Chen, Y. Wang, R. Luo, B. Li, Z. Chen, Y. Pan, Preparation and thermal insulation analysis of SiC_w-SiC foam with hollow skeletons via carbon foam template CVI method, Mater. Char. 134 (2017) 296–301, https://doi.org/10.1016/j.matchar.2017.11.014.
[3] S. Yu, Z. Chen, Y. Wang, R. Luo, Y. Pan, A study of thermal insulation properties and microstructure of ultra-light 3D-carbon foam via direct carbonization of polymer foam, J. Porous Mater. 25 (2018) 527–536, https://doi.org/10.1007/s10934-017-0465-3.
[4] H.G. Shi, T. Wang, J.B. Cheng, H.B. Zhao, S.L. Li, Y.Z. Wang, Ultralow-density carbon foam composites with bean-like Co-embedded carbon nanotube whiskers towards high-performance microwave absorption, J. Alloys Compd. 863 (2021) 158090, https://doi.org/10.1016/j.jallcom.2020.158090.
[5] K.W. Stahlfeld, E.L. Belmont, Carbon foam production from lignocellulosic biomass via high pressure pyrolysis, J. Anal. Appl. Pyrolysis 156 (2021) 105115, https://doi.org/10.1016/j.jaap.2021.105115.
[6] M.V.G. Zimmermann, D. Perondi, L.K. Lazzari, M. Godinho, A.J. Zattera, Carbon foam production by biomass pyrolysis, J. Porous Mater. 27 (2020) 1119–1125, https://doi.org/10.1007/s10934-020-00888-y.
[7] Z. Yu, D. Feng, Y. Feng, X. Zhang, Thermal conductivity and energy storage capacity enhancement and bottleneck of shape-stabilized phase change composites with graphene foam and carbon nanotubes, Compos. Part A Appl. Sci. Manuf. 152 (2022) 106703, https://doi.org/10.1016/j.compositesa.2021.106703.
[8] A. Chithra, P. Wilson, S. Vijayan, R. Rajeev, K. Prabhakaran, Carbon foams with low thermal conductivity and high EMI shielding effectiveness from sawdust, Ind. Crops Prod. 145 (2020) 112076, https://doi.org/10.1016/j.indcrop.2019.112076.
[9] P. Gao, A. Wang, X. Wang, T. Zhang, Synthesis of highly ordered Ir-containing mesoporous carbon materials by organic–organic self-assembly, Chem. Mater. 20 (5) (2008) 1881–1888, https://doi.org/10.1021/cm702815e.
[10] S. Hu, Y. Li, Polyols and polyurethane foams from base-catalyzed liquefaction of lignocellulosic biomass by crude glycerol: effects of crude glycerol impurities, Ind. Crops Prod. 57 (2014) 188–194, https://doi.org/10.1016/j.indcrop.2014.03.032.
[11] P. Jana, V. Fierro, A. Pizzi, A. Celzard, Biomass-derived, thermally conducting, carbon foams for seasonal thermal storage, Biomass Bioenergy 67 (2014) 312–318, https://doi.org/10.1016/j.biombioe.2014.04.031.
[12] T. Kyotani, Control of pore structure in carbon, Carbon 38 (2) (2000) 269–286, https://doi.org/10.1016/S0008-6223(99)00142-6.
[13] M.L. Lin, C.C. Huang, M.Y. Lo, C.Y. Mou, Well-ordered mesoporous carbon thin film with perpendicular channels: application to direct methanol fuel cell, J. Phys. Chem. C 112 (3) (2008) 867–873, https://doi.org/10.1021/jp076748m.
[14] J. Sánchez-Martín, J. Beltrán-Heredia, A. Delgado-Regaña, M.A. Rodríguez-González, F. Rubio-Alonso, Optimization of tannin rigid foam as adsorbents for wastewater treatment, Ind. Crops Prod. 49 (2013) 507–514, https://doi.org/10.1016/j.indcrop.2013.05.029.
[15] Z. Wu, D. Zhao, Ordered mesoporous materials as adsorbents, Chem. Comm. 47 (12) (2011) 3332–3338, https://doi.org/10.1039/C0CC04909C.
[16] A.S. Yargic, G. Gunduz Meric, R.Z. Yarbay, N. Ozbay, Investigation of CO_2 sequestration performance and statistical analysis of dye removal efficiency of liquefied hornbeam based carbon foams: effects of biomass/solvent weight ratio, tar contribution, and chemical activation, Mater. Today Sustain. 24 (2023) 100517, https://doi.org/10.1016/j.mtsust.2023.100517.
[17] J. Zhou, X. Yuan, W. Xing, W.J. Si, S.P. Zhuo, Mesoporous carbons derived from citrates for use in electrochemical capacitors, Carbon 49 (3) (2011) 1054, https://doi.org/10.1016/j.carbon.2010.10.043, 1054.
[18] B. Tsyntsarski, B. Petrova, T. Budinova, N. Petrov, L.F. Velasco, J.B. Parra, C. O. Ania, Porosity development during steam activation of carbon foams from chemically modified pitch, Microporous Mesoporous Mater. 154 (2012) 56–61, https://doi.org/10.1016/j.micromeso.2011.08.023.
[19] M. Liu, L. Gan, F. Zhao, X. Fan, H. Xu, F. Wu, Z. Xu, Z. Hao, L. Chen, Carbon foams with high compressive strength derived from polyarylacetylene resin, Carbon 45 (15) (2007) 3055–3057, https://doi.org/10.1016/j.carbon.2007.10.003.
[20] X. Wang, J. Zhong, Y. Wang, M. Yu, Y. Wang, The study on the formation of graphitic foam, Mater. Lett. 61 (3) (2007) 741–746, https://doi.org/10.1016/j.matlet.2006.05.052.

[21] M. Calvo, R. García, A. Arenillas, I. Suárez, S.R. Moinelo, Carbon foams from coals. A preliminary study, Fuel 84 (17) (2005) 2184–2189, https://doi.org/10.1016/j.fuel.2005.06.008.

[22] Y. Chen, B.Z. Chen, X.C. Shi, H. Xu, Y.J. Hu, Y. Yuan, N.B. Shen, Preparation of pitch-based carbon foam using polyurethane foam template, Carbon 45 (10) (2007) 2132–2134. https://10.1016/j.carbon.2007.06.004.

[23] A. Yadav, R. Kumar, G. Bhatia, G.L. Verma, Development of mesophase pitch derived high thermal conductivity graphite foam using a template method, Carbon 49 (11) (2011) 3622–3630, https://doi.org/10.1016/j.carbon.2011.04.065.

[24] Y. Ren, Q. Xu, J. Zhang, H. Yang, B. Wang, D. Yang, J. Hu, Z. Liu, Functionalization of biomass carbonaceous aerogels: selective preparation of MnO_2@CA composites for supercapacitors, ACS Appl. Mater. Interfaces 6 (12) (2014) 9689–9697, https://doi.org/10.1021/am502035g.

[25] R.C.S. Araújo, V.M.D. Pasa, B.N. Melo, Effects of biopitch on the properties of flexible polyurethane foams, Eur. Polym. J. 41 (6) (2005) 1420–1428, https://doi.org/10.1016/j.eurpolymj.2004.12.021.

[26] E. Ekinci, Turkish oil shales potential for synthetic crude oil and carbon materials production, International Conference on Oil Shale: "Recent Trends in Oil Shale", 7-9 November 2006, Amman, Jordan.

[27] R.V.R.A. Rios, M. Martinez-Escandell, M. Molina-Sabio, F. Rodriguez-Reinoso, Carbon foam prepared by pyrolysis of olive stones under steam, Carbon 44 (8) (2006) 1448–1454, https://doi.org/10.1016/j.carbon.2005.11.028.

[28] M.W. Smith, B. Pecha, G. Helms, L. Scudiero, M. Garcia-Perez, Chemical and morphological evaluation of chars produced from primary biomass constituents: cellulose, xylan, and lignin, Biomass Bioenergy 104 (2017) 17–35, https://doi.org/10.1016/j.biombioe.2017.05.015.

[29] N. Ozbay, A.S. Yargic, Carbon foam production from bio-based polyols of liquefied spruce tree sawdust: effects of biomass/solvent mass ratio and pyrolytic oil addition, J. Appl. Polym. Sci. 136 (11) (2019) 47185, https://doi.org/10.1002/app.47185.

[30] S. Liu, Z. Huang R. Wang, A carbon foam with a bimodal micro–mesoporous structure prepared from larch sawdust for the gas-phase toluene adsorption, Mater. Res. Bull. 48 (7) (2013) 2437–2441, https://doi.org/10.1016/j.materresbull.2013.02.069.

[31] R. Wang, W. Li, S. Liu, A porous carbon foam prepared from liquefied birch sawdust, J. Mater. Sci. 47 (2012) 1977–1984, https://doi.org/10.1007/s10853-011-5993-7.

[32] A.S. Yargic, N. Ozbay, Effect of chemical activation on the cellular structure of biopitch-derived green carbon foam, Diam. Relat. Mater. 96 (2019) 58–66, https://doi.org/10.1016/j.diamond.2019.04.032.

[33] A.Ş. Yargıç, G.G. Meriç, N. Özbay, The soft template-assisted foaming technique's impact on biopitch-based porous carbon foam features, Ind. Crops Prod. 224 (2025) 120320, https://doi.org/10.1016/j.indcrop.2024.120320.

[34] T. Hlabathe, N. Shiba, X. Liu, Mesophase pitch derived carbon foams with high compressive strengths and thermal conductivities as cobalt support, Mater. Today Commun. 35 (2023) 105537, https://doi.org/10.1016/j.mtcomm.2023.105537.

[35] L.V. Daza Serna, J.C. Solarte Toro, S. Serna Loaiza, Y. Chacón Perez, C.A. Cardona Alzate, Agricultural waste management through energy producing biorefineries: the Colombian case, Waste Biomass Valori 7 (2016) 789–798, https://doi.org/10.1007/s12649-016-9576-3.

[36] H. Zhang, Y. Yan, L. Yang, Preparation of activated carbon from sawdust by zinc chloride activation, Adsorption 16 (2010) 161–166, https://doi.org/10.1007/s10450-010-9214-5.

[37] N. Asim, M. Badiei, M.A. Alghoul, M. Mohammad, A. Fudholi, M. Akhtaruzzaman, N. Amin, K. Sopian, Biomass and industrial wastes as resource materials for aerogel preparation: opportunities, challenges, and research directions, Ind. Eng. Chem. Res. 58 (38) (2019) 17621–17645, https://doi.org/10.1021/acs.iecr.9b02661.

[38] P.T. Nguyen, N.H. Do, X.Y. Goh, C.J. Goh, R.H. Ong, P.K. Le, N. Phan-Thien, H. M. Duong, Recent progresses in eco-friendly fabrication and applications of sustainable aerogels from various waste materials, Waste Biomass Valori (2022) 1–23, https://doi.org/10.1007/s12649-021-01627-3.

[39] M.A. Aslam, W. Ding, S. ur Rehman, A. Hassan, Y. Bian, Q. Liu, Z. Sheng, Low cost 3D bio-carbon foams obtained from wheat straw with broadened bandwidth electromagnetic wave absorption performance, Appl. Surf. Sci. 543 (2021) 148785, https://doi.org/10.1016/j.apsusc.2020.148785.

[40] F. Yang, S. Zhang, Y. Sun, K. Cheng, J. Li, D.C. Tsang, Fabrication and characterization of hydrophilic corn stalk biochar-supported nanoscale zero-valent iron composites for efficient metal removal, Bioresour. Technol. 265 (2018) 490–497, https://doi.org/10.1016/j.biortech.2018.06.029.

[41] D. Khalafallah, X. Quan, C. Ouyang, M. Zhi, Z. Hong, Heteroatoms doped porous carbon derived from waste potato peel for supercapacitors, Renew. Energy 170 (2021) 60–71, https://doi.org/10.1016/j.renene.2021.01.077.

[42] H. Gu, Y. Xu, Y. Shen, P. Zhu, T. Zhao, Y. Hu, R. Sun, C.P. Wong, Versatile biomass carbon foams for fast oil–water separation, flexible pressure-strain sensors, and electromagnetic interference shielding, Ind. Eng. Chem. Res. 59 (47) (2020) 20740–20748, https://doi.org/10.1021/acs.iecr.0c04316.

[43] X. Hu, H. Huang, Y. Hu, X. Lu, Y. Qin, Novel bio-based composite phase change materials with reduced graphene oxide-functionalized spent coffee grounds for efficient solar-to-thermal energy storage, Sol. Energy Mater. Sol. Cells 219 (2021) 110790, https://doi.org/10.1016/j.solmat.2020.110790.

[44] R.W.I.B. Priyadarshana, P.E. Kaliyadasa, S.R.W.M.C.J.K. Ranawana, K.G. C. Senarathna, Biowaste management: banana fiber utilization for product development, J. Nat. Fibers 19 (4) (2022) 1461–1471, https://doi.org/10.1080/15440478.2020.1776665.

[45] J. Zhang, J. Xiang, Z. Dong, Y. Liu, Y. Wu, C. Xu, G. Du, Biomass derived activated carbon with 3D connected architecture for rechargeable lithium−sulfur batteries, Electrochim. Acta 116 (2014) 146–151, https://doi.org/10.1016/j.electacta.2013.11.035.

[46] M. Khalid, R. Paul, A.M. Honorato, H. Varela, Pinus nigra pine derived hierarchical carbon foam for high performance supercapacitors, J. Electroanal. Chem. 863 (2020) 114053, https://doi.org/10.1016/j.jelechem.2020.114053.

[47] C. Sun, X. Li, Z. Cai, F. Ge, Carbonized cotton fabric in-situ electrodeposition polypyrrole as high-performance flexible electrode for wearable supercapacitor, Electrochim. Acta 296 (2019) 617–626, https://doi.org/10.1016/j.electacta.2018.11.045.

[48] C. Zequine, C.K. Ranaweera, Z. Wang, S. Singh, P. Tripathi, O.N. Srivastava, B. K. Gupta, K. Ramasamy, P.K. Kahol, P.R. Dvornic, R.K. Gupta, High performance and flexible supercapacitors based on carbonized bamboo fibers for wide temperature applications, Sci. Rep. 6 (1) (2016) 31704, https://doi.org/10.1038/srep31704.

[49] H. Li, P. Su, Q. Liao, Y. Liu, Y. Li, X. Niu, X. Liu, K. Wang, Olive leaves-derived hierarchical porous carbon as cathode material for anti-self-discharge zinc-ion hybrid capacitor, Small 19 (49) (2023) 2304172, https://doi.org/10.1002/smll.202304172.

[50] Z. Nie, Y. Wang, X. Li, R. Wang, Y. Zhao, H. Song, H. Wang, Heteroatom-doped hierarchical porous carbon from corn straw for high-performance supercapacitor, J. Energy Storage 44 (2021) 103410, https://doi.org/10.1016/j.est.2021.103410.

[51] R. Wang, X. Li, J. Yang, M. Yang, H. Song, Y. Zhao, H. Wang, A novel sustainable cornstalk-derived porous carbon composited with in-situ polymerized polyaniline nanowires for high-performance asymmetric supercapacitors, J. Energy Storage 68 (2023) 107764, https://doi.org/10.1016/j.est.2023.107764.

[52] W. Li, Z. Huang, Y. Wu, X. Zhao, S. Liu, Honeycomb carbon foams with tunable pore structures prepared from liquefied larch sawdust by self-foaming, Ind. Crops Prod. 64 (2015) 215–223, https://doi.org/10.1016/j.indcrop.2014.09.043.

[53] A.Ş. Yargıç, R.Z.Y. Şahin, N. Özbay, Investigation of solvent type effect on the structural properties of bio-polyol-based carbon foam, J. Fac. Eng. Archit. Gazi Univ. 36 (1) (2021) 133–145, https://doi.org/10.17341/gazimmfd.673657.

[54] A.Ş. Yargıç, G. Gündüz Meriç, Y. Dolaş, N. Özbay, Production and characterization of open-celled carbon foams from sawmill waste, bilecik Seyh Edebali univ, J. Sci. 8 (2) (2021) 1044–1056, https://doi.org/10.35193/bseufbd.1013724.

[55] B.B. Uzun, E. Apaydin-Varol, F. Ateş, N. Özbay, A.E. Pütün, Synthetic fuel production from tea waste: characterisation of bio-oil and bio-char, Fuel 89 (1) (2010) 176–184, https://doi.org/10.1016/j.fuel.2009.08.040.

[56] R.C.S. Araujo, V.M.D. Pasa, Mechanical and thermal properties of polyurethane elastomers based on hydroxyl-terminated polybutadienes and biopitch, J. Appl. Polym. Sci. 88 (3) (2003) 759–766, https://doi.org/10.1002/app.11526.

[57] R.C.S. Araújo, V.M.D. Pasa, New Eucalyptus tar-derived polyurethane coatings, Prog. Org. Coating 51 (1) (2004) 6–14, https://doi.org/10.1016/j.porgcoat.2004.04.002.

[58] M.J. Prauchner, V.M. Pasa, S.M. de Menezes, Solid-state ^{13}C NMR quantitative study of Eucalyptus tar pitches, J. Wood Chem. Technol. 21 (4) (2001) 371–385, https://doi.org/10.1081/WCT-100108332.

[59] M.J. Prauchner, V.M. Pasa, C. Otani, S. Otani, S.M. de Menezes, Eucalyptus tar pitch pretreatment for carbon material processing, J. Appl. Polym. Sci. 91 (3) (2004) 1604–1611, https://doi.org/10.1002/app.13298.

[60] J. Rocha, A. Countinho, C. Luengo, Biopitch produced from Eucalyptus wood pyrolysis liquids as a renewable binder for carbon electrode manufacture, Braz. J. Chem. Eng. (2002) 127–132, https://doi.org/10.1590/S0104-66322002000200002.

[61] A.S. Yargic, Conversion of biopitch to carbon foam with tunable properties: the role of chemical activation, in: D. Kavak (Ed.), Current Engineering Sciences Research, Livre de Lyon, Lyon, 2021, pp. 1–22. Chapter-1.

[62] A.Ş. Yargıç, Production and Characterization of Carbon Foam, Doctor of Philosophy, Department of Chemical Engineering, Bilecik Seyh Edebali University and Anadolu University Joint Postgraduate Education Program, Bilecik, Turkey, 2017.

[63] M.J. Prauchner, V.M. Pasa, C. Otani, S. Otani, Characterization and thermal polymerization of Eucalyptus tar pitches, Energy Fuels 15 (2) (2001) 449–454, https://doi.org/10.1021/ef000196o.

[64] P.H. Gamlen, J.W. White, Structure and dynamics of microcrystalline graphite, graphon, by neutron scattering, Chem. Soc., Faraday trans. II: Mol. Chem. Phys. 72 (1976) 446–455, https://doi.org/10.1039/F29767200446.

[65] B.N. Melo, V.M. Pasa, Composites based on eucalyptus tar pitch/castor oil polyurethane and short sisal fibers, J. Appl. Polym. Sci. 89 (14) (2003) 3797–3802, https://doi.org/10.1002/app.12424.

[66] M.J. Jeon, J.K. Jeon, D.J. Suh, S.H. Park, Y.J. Sa, S.H. Joo, Y.K. Park, Catalytic pyrolysis of biomass components over mesoporous catalysts using Py-GC/MS, Catal. Today 204 (2013) 170–178, https://doi.org/10.1016/j.cattod.2012.07.039.

[67] N. Ozbay, A.S. Yargic, R.Z.Y. Sahin, E. Yaman, Valorization of banana peel waste via in-situ catalytic pyrolysis using Al-Modified SBA-15, Renew. Energy 140 (2019) 633–646, https://doi.org/10.1016/j.renene.2019.03.071.

[68] K.S. Lakhi, D.H. Park, G. Singh, S.N. Talapaneni, U. Ravon, K. Al-Bahily, A. Vinu, Energy efficient synthesis of highly ordered mesoporous carbon nitrides with uniform rods and their superior CO_2 adsorption capacity, Mater. Chem. A. 5 (31) (2017) 16220–16230, https://doi.org/10.1039/C6TA10716H.

[69] Y. Chen, Y. Huang, J. Xiu, X. Han, X. Bao, Direct synthesis, characterization and catalytic activity of titanium-substituted SBA-15 mesoporous molecular sieves,

Appl. Catal. A: Gen. 273 (1–2) (2004) 185–191, https://doi.org/10.1016/j.apcata.2004.06.030.
[70] N. Wang, X. Yu, Y. Wang, W. Chu, M. Liu, A comparison study on methane dry reforming with carbon dioxide over $LaNiO_3$ perovskite catalysts supported on mesoporous SBA-15, MCM-41 and silica carrier, Catal. Today 212 (2013) 98–107, https://doi.org/10.1016/j.cattod.2012.07.022.
[71] Y. Zhang, R. Xiao, X. Gu, H. Zhang, D. Shen, G. He, Catalytic pyrolysis of biomass with Fe/La/SBA-15 catalyst using TGA–FTIR analysis, Bioresources 9 (3) (2014) 5234–5245, https://doi.org/10.15376/biores.9.3.5234-5245.
[72] B. Tsyntsarski, B. Petrova, T. Budinova, N. Petrov, M. Krzesinska, S. Pusz, J. Majewska, P. Tzvetkov, Carbon foam derived from pitches modified with mineral acids by a low pressure foaming process, Carbon 48 (12) (2010) 3523–3530, https://doi.org/10.1016/j.carbon.2010.05.048.
[73] T. Beechem, K. Lafdi, A. Elgafy, Bubble growth mechanism in carbon foams, Carbon 43 (5) (2005) 1055–1064, https://doi.org/10.1016/j.carbon.2004.11.046.
[74] Y. Yuan, Z. Qin, Z. Xu, SBA-15 templated mesoporous MnO_x for catalytic ozonation of toluene, Catal. Lett. 150 (2020) 365–374, https://doi.org/10.1007/s10562-019-03000-5.
[75] H. Seidel, L. Csepregi, A. Heuberger, H. Baumgärtel, Anisotropic etching of crystalline silicon in alkaline solutions: I. Orientation dependence and behavior of passivation layers, J. Electrochem. Soc. 137 (11) (1990) 3612, https://doi.org/10.1149/1.2086277.
[76] J. Shi, X. Jiang, J. Sun, B. Ban, J. Li, J. Chen, Recycled silicon-based anodes with three-dimensional hierarchical porous carbon framework synthesized by a self-assembly $CaCO_3$ template method for lithium ion battery, J. Alloys Compd. 858 (2021) 157703, https://doi.org/10.1016/j.jallcom.2020.157703.
[77] B.K. Gale, Wet etching and bulk micromachining, fundamentals of micromachining lecture notes. https://my.mech.utah.edu/~gale/mems/Lecture%2010%20Wet%20Etching.pdf, 2002. (Accessed 16 October 2023).
[78] E.D. Palik, V.M. Bermudez, O.J. Glembocki, Ellipsometric study of orientation-dependent etching of silicon in aqueous KOH, J. Electrochem. Soc. 132 (4) (1985) 871, https://doi.org/10.1149/1.2113976.
[79] E.D. Palik, H.F. Gray, P.B. Klein, A Raman study of etching silicon in aqueous KOH, J. Electrochem. Soc. 130 (4) (1983) 956, https://doi.org/10.1149/1.2119866.
[80] A.H. Basta, V. Fierro, H. El-Saied, A. Celzard, 2-Steps KOH activation of rice straw: an efficient method for preparing high-performance activated carbons, Bioresour. Technol. 100 (17) (2009) 3941–3947, https://doi.org/10.1016/j.biortech.2009.02.028.
[81] A.L. Cazetta, A.M. Vargas, E.M. Nogami, M.H. Kunita, M.R. Guilherme, A. C. Martins, T.L. Silva, J.C.G. Moraes, V.C. Almeida, NaOH-activated carbon of high surface area produced from coconut shell: kinetics and equilibrium studies from the methylene blue adsorption, Chem. Eng. J. 174 (1) (2011) 117–125, https://doi.org/10.1016/j.cej.2011.08.058.
[82] F.C. Wu, R.L. Tseng, R.S. Juang, Preparation of highly microporous carbons from fir wood by KOH activation for adsorption of dyes and phenols from water, Sep. Purif. Technol. 47 (1–2) (2005) 10–19, https://doi.org/10.1016/j.seppur.2005.03.013.
[83] G. Tondi, A. Pizzi, L. Delmotte, J. Parmentier, R. Gadiou, Chemical activation of tannin–furanic carbon foams, Ind. Crops Prod. 31 (2) (2010) 327–334, https://doi.org/10.1016/j.indcrop.2009.11.013.
[84] J. Wang, S. Kaskel, KOH activation of carbon-based materials for energy storage, J. Mater. Chem. 22 (45) (2012) 23710–23725, https://doi.org/10.1039/C2JM34066F.
[85] E. Apaydın-Varol, Y. Erülken, A study on the porosity development for biomass based carbonaceous materials, J. Taiwan Inst. Chem. Eng. 54 (2015) 37–44, https://doi.org/10.1016/j.jtice.2015.03.003.
[86] Y. Sun, P.A. Webley, Preparation of activated carbons with large specific surface areas from biomass corncob and their adsorption equilibrium for methane, carbon dioxide, nitrogen, and hydrogen, Ind. Eng. Chem. Res. 50 (15) (2011) 9286–9294, https://doi.org/10.1021/ie1024003.
[87] F. Ning, W. Cong, Y. Hu, H. Wang, Additive manufacturing of carbon fiber-reinforced plastic composites using fused deposition modeling: effects of process parameters on tensile properties, J. Compos. Mater. 51 (4) (2017) 451–462, https://doi.org/10.1177/0021998316646169.
[88] J.W. Shim, S.J. Park, S.K. Ryu, Effect of modification with HNO_3 and NaOH on metal adsorption by pitch-based activated carbon fibers, Carbon 39 (11) (2001) 1635–1642, https://doi.org/10.1016/S0008-6223(00)00290-6.
[89] R.L. Tseng, Mesopore control of high surface area NaOH-activated carbon, J. Colloid Interface Sci. 303 (2) (2006) 494–502, https://doi.org/10.1016/j.jcis.2006.08.024.
[90] C. Chen, E.B. Kennel, A.H. Stiller, P.G. Stansberry, J.W. Zondlo, Carbon foam derived from various precursors, Carbon 44 (8) (2006) 1535–1543, https://doi.org/10.1016/j.carbon.2005.12.021.
[91] F. Kurosaki, H. Koyanaka, M. Tsujimoto, Y. Imamura, Shape-controlled multi-porous carbon with hierarchical micro–meso-macro pores synthesized by flash heating of wood biomass, Carbon 46 (6) (2008) 850–857, https://doi.org/10.1016/j.carbon.2008.02.014.
[92] S.S.R. Dehkordi, Q. Delavar, H.A. Ebrahim, S.S. Partash, CO_2 adsorption by coal-based activated carbon modified with sodium hydroxide, Mater. Today Commun. 33 (2022) 104776, https://doi.org/10.1016/j.mtcomm.2022.104776.
[93] B.S. Girgis, S.S. Yunis, A.M. Soliman, Characteristics of activated carbon from peanut hulls in relation to conditions of preparation, Mater. Lett. 57 (1) (2002) 164–172, https://doi.org/10.1016/S0167-577X(02)00724-3.
[94] F.A. Lopez, T.A. Centeno, I. Garcia-Diaz, F.J. Alguacil, Textural and fuel characteristics of the chars produced by the pyrolysis of waste wood, and the properties of activated carbons prepared from them, J. Anal. Appl. Pyrolysis 104 (2013) 551–558, https://doi.org/10.1016/j.jaap.2013.05.014.
[95] M.S.H.K. Tushar, N. Mahinpey, A. Khan, H. Ibrahim, P. Kumar, R. Idem, Production, characterization and reactivity studies of chars produced by the isothermal pyrolysis of flax straw, Biomass Bioenergy 37 (2012) 97–105, https://doi.org/10.1016/j.biombioe.2011.12.027.
[96] S. Zhang, M. Zheng, Z. Lin, N. Li, Y. Liu, B. Zhao, H. Pang, J. Cao, P. He, Y. Shi, Activated carbon with ultrahigh specific surface area synthesized from natural plant material for lithium–sulfur batteries, J. Mater. Chem. A 2 (38) (2014) 15889–15896, https://doi.org/10.1039/C4TA03503H.
[97] M.J. Prauchner, V.M. Pasa, N.D. Molhallem, C. Otani, S. Otani, L.C. Pardini, Structural evolution of Eucalyptus tar pitch-based carbons during carbonization, Biomass Bioenergy 28 (1) (2005) 53–61, https://doi.org/10.1016/j.biombioe.2004.05.004.
[98] M.X. Wang, C.Y. Wang, T.Q. Li, Z.J. Hu, Preparation of mesophase-pitch-based carbon foams at low pressures, Carbon 46 (1) (2008) 84–91, https://doi.org/10.1016/j.carbon.2007.10.038.
[99] J. Fayos, Possible 3D carbon structures as progressive intermediates in graphite to diamond phase transition, J. Solid State Chem. 148 (2) (1999) 278–285, https://doi.org/10.1006/jssc.1999.8448.
[100] H. Lipson, A.R. Stokes, A new structure of carbon, Nature 149 (3777) (1942) 328, https://doi.org/10.1038/149328a0, 328.
[101] M.S. Strano, A.L. Zydney, H. Barth, G. Wooler, H. Agarwal, H.C. Foley, Ultrafiltration membrane synthesis by nanoscale templating of porous carbon, J. Membr. Sci. 198 (2) (2002) 173–186, https://doi.org/10.1016/S0376-7388(01)00574-9.
[102] X. Luo, A. Mohanty, M. Misra, Lignin as a reactive reinforcing filler for water-blown rigid biofoam composites from soy oil-based polyurethane, Ind. Crops Prod. 47 (2013) 13–19, https://doi.org/10.1016/j.indcrop.2013.01.040.
[103] M. Inagaki, J. Qiu, Q. Guo, Carbon foam: preparation and application, Carbon 87 (2015) 128–152, https://doi.org/10.1016/j.carbon.2015.02.021.
[104] S. Lei, Q. Guo, L. Liu, Preparation of phenolic-based carbon foam with controllable pore structure and high compressive strength, Carbon 15 (3) (2010) 2644–2646, https://doi.org/10.1016/j.carbon.2010.03.017.
[105] J. Nicholson, C. Thomas, Syntactic carbon foams, Carbon (1973) 65–66, https://doi.org/10.1016/0008-6223(73)90009-2.
[106] R.A. Mercuri, T.R. Wessendorf, J.M. Criscione, Carbon foam: its preparation and properties, Am. Chem. Soc. Div. Pet. Chem. Prepr 12 (4) (1968).
[107] N. Gallego, J. Klett, Carbon foams for thermal management, Carbon 41 (2003) 1461–1466, https://doi.org/10.1016/S0008-6223(03)00091-5.
[108] J. Klett, Process for Making Carbon Foam, US, Patent No. 6033506, 2000.
[109] J. Klett, Pitch-Based Carbon Foam and Composites, US, Patent No. 6261485, 2001.
[110] E. Kılıç, Preparation and characterization of graphene-based green nanocomposites and their utilization in various applications. Doctor of Philosophy, Department of Chemistry, Hacettepe University, Ankara, Turkey, 2019.
[111] D. Kang, J.W. Lee, Enhanced methane decomposition over nickel–carbon–B_2O_3 core–shell catalysts derived from carbon dioxide, Appl. Catal. B Environ. 186 (2016) 41–55, https://doi.org/10.1016/j.apcatb.2015.12.045.
[112] S. Li, Y. Tian, Y. Zhong, X. Yan, Y. Song, Q. Guo, J. Shi, L. Liu, Formation mechanism of carbon foams derived from mesophase pitch, Carbon 49 (2) (2011) 618–624, https://doi.org/10.1016/j.carbon.2010.10.007.
[113] X. He, N. Zhang, X. Shao, M. Wu, M. Yu, J. Qiu, A layered-template-nanospace-confinement strategy for production of corrugated graphene nanosheets from petroleum pitch for supercapacitors, Chem. Eng. J. 297 (2016) 121–127, https://doi.org/10.1016/j.cej.2016.03.153.